NASA TECHNICAL NOTE

NASA TN D-6625
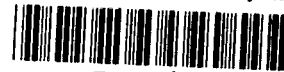
EFFECTS OF NORMAL ACCELERATION ON TRANSIENT BURNING-RATE AUGMENTATION OF AN ALUMINIZED SOLID PROPELLANT

by G. Burton Northam

Langley Research Center
Hampton, Va. 23365

1. Report No. NASA TN D-6625	2. Government Accession No.	3. Recipient's Catalog No.
4. Title and Subtitle EFFECTS OF NORMAL ACCELERATION ON TRANSIENT BURNING-RATE AUGMENTATION OF AN ALUMINIZED SOLID PROPELLANT		5. Report Date April 1972
		6. Performing Organization Code
7. Author(s) G. Burton Northam		8. Performing Organization Report No. L-7847
9. Performing Organization Name and Address NASA Langley Research Center Hampton, Va. 23365		10. Work Unit No. 113-32-04-03
		11. Contract or Grant No.
12. Sponsoring Agency Name and Address National Aeronautics and Space Administration Washington, D.C. 20546		13. Type of Report and Period Covered Technical Note
		14. Sponsoring Agency Code

15. Supplementary Notes   The information presented herein was included in a thesis entitled "Acceleration-Induced Transient Burning-Rate Augmentation of an Aluminized Solid Rocket Propellant" submitted in partial fulfillment of the requirements for the degree of Doctor of Philosophy in Mechanical Engineering, Virginia Polytechnic Institute, Blacksburg, Virginia, June 1969.

16. Abstract

Instantaneous burning-rate data for a polybutadiene acrylic acid (PBAA) propellant, containing 16 weight percent aluminum, were calculated from the pressure histories of a test motor with 96.77 cm^2 (15 in^2) of burning area and a 5.08-cm-thick (2.0 in.) propellant web. Additional acceleration tests were conducted with reduced propellant web thicknesses of 3.81, 2.54, and 1.27 cm (1.5, 1.0, and 0.5 in.). The metallic residue collected from the various web thickness tests was characterized by weight and shape and correlated with the instantaneous burning-rate measurements. Rapid-depressurization extinction tests were conducted in order that surface pitting characteristics due to localized increased burning rate could be correlated with the residue analysis and the instantaneous burning-rate data.

The acceleration-induced burning-rate augmentation was strongly dependent on propellant distance burned, or burning time, and thus was transient in nature. The results from the extinction tests and the residue analyses indicate that the transient rate augmentation was highly dependent on local enhancement of the combustion zone heat feedback to the surface by the growth of molten residue particles on or just above the burning surface. The size, shape, and number density of molten residue particles, rather than the total residue weight, determined the acceleration-induced burning-rate augmentation.

17. Key Words (Suggested by Author(s)) Acceleration Propellant burning rate Spin-stabilized rockets	18. Distribution Statement Unclassified – Unlimited		
19. Security Classif. (of this report) Unclassified	20. Security Classif. (of this page) Unclassified	21. No. of Pages 56	22. Price* $3.00

EFFECTS OF NORMAL ACCELERATION ON TRANSIENT BURNING-RATE AUGMENTATION OF AN ALUMINIZED SOLID PROPELLANT*

By G. Burton Northam
Langley Research Center

SUMMARY

This paper presents experimental results on the transient burning-rate augmentation of a polybutadiene acrylic acid (PBAA) propellant, containing 16 weight percent aluminum, burned in a 5.08-cm (2.0 in.) web slab motor at pressure levels from 2.07 to 8.27 MN/m² (300 to 1200 psia) with normal centrifugal accelerations from 0g to 140g. The metallic residue retained in similar motors with incremental propellant web thicknesses was correlated with (1) the burning-rate data and (2) geometrical characterizations of the pitted propellant surface obtained from extinction tests at different burn times and acceleration levels.

The normal-acceleration-induced burning-rate augmentation at a given pressure was strongly dependent on (1) acceleration level and (2) distance of propellant burned (or burning time). This transient rate augmentation was caused by increased localized burning rates resulting from local enhancement of the combustion zone heat transfer to the surface by the growth of molten residue particles retained just above the burning surface. The transient size, shape, and number density of the particles on the surface, rather than the total residue weight, determined the acceleration-induced burning-rate augmentation.

INTRODUCTION

Many solid-propellant rocket vehicles have been developed that use spin for inertial stabilization and for reducing dispersion due to thrust misalinement in flight. Spin-induced effects on some rocket motors with metallized propellants have led to increases in propellant burning rate, motor chamber pressure, and chamber heating. These phenomena are the result of centrifugal loading effects on the combustion process and spin-induced vortex flow effects in the combustion chamber and nozzle.

---

*The information presented herein was included in a thesis entitled "Acceleration-Induced Transient Burning-Rate Augmentation of an Aluminized Solid Rocket Propellant" submitted in partial fulfillment of the requirements for the degree of Doctor of Philosophy in Mechanical Engineering, Virginia Polytechnic Institute, Blacksburg, Virginia, June 1969.

From a review of the literature (refs. 1 to 14), several qualitative statements can be made concerning the effects of aluminized propellant formulation variables and ballistics on the sensitivity of the propellant burning rate to acceleration environments:

(1) The burning-rate augmentation varies with acceleration level depending on the propellant and is a strong function of the orientation of the acceleration vector. This effect is largest when the acceleration vector is normal into the burning surface.

(2) Although the rate augmentation generally decreases with decreased aluminum particle size and aluminum percentage, in many cases it depends on the propellant system and acceleration level. Reduction of the oxidizer particle size also decreases the burning-rate augmentation.

(3) No consistent pressure dependence of rate augmentation was observed for the wide variety of propellants that have been tested.

(4) The propellant static test burning rate appears to be the best index for predicting the sensitivity of solid propellants to acceleration loads.

(5) The rate augmentation is transient and, thus, also varies with burning time or propellant distance burned.

To date the characterization of the transient rate augmentation has been limited by one or more of the following experimental and analytical constraints: (a) the use of small propellant strands which produce unrealistic edge effects, (b) the use of thin-web test motors that do not have sufficient propellant web thickness to allow the rate augmentation to reach a quasi-equilibrium value, and (c) the use of long time-average augmentation as a measure of the effect.

The subject investigation was conducted to characterize the transient burning-rate augmentation of an aluminized composite solid propellant subject to acceleration forces normal into the burning surface and to elucidate the mechanisms of burning-rate augmentation due to the imposed acceleration force. Since previous results (refs. 3 and 11) indicated increased weights of metallic residue with increasing acceleration level, particular attention was directed toward correlation of the calculated instantaneous rate data with the metallic fuel residue remaining at motor burnout. The propellant web thickness was varied in order that this residue could be collected and correlated with distance of propellant burned.

SYMBOLS

Values are given in both SI and U.S. Customary Units. The measurements and calculations were made in U.S. Customary Units.

A   growth constant in equation (4)

A_t throat area

a   burning-rate constant

DB   distance burned

$d_{t,f}$ final throat diameter

$d_{t,i}$ initial throat diameter

K   ratio of burning surface to throat area

n   pressure exponent

p   pressure

$\bar{p}$ average pressure

p_{ref} reference pressure in rate equation

p_t instantaneous chamber pressure

r   burning rate

$\bar{r}$ average burning rate

r/r_0 burning-rate augmentation, $\dfrac{\text{Rate under acceleration}}{\text{Static rate at same pressure}}$

r_0 static test burning rate

r_t instantaneous burning rate

$r_{t,max}$ maximum instantaneous burning rate

t   time

t_b pressure burn time

t_i	initial time to burn time
W	residue weight
w	specific residue weight, $\dfrac{\text{Total residue weight}}{\text{Burning surface area}}$
α_n	normal acceleration into burning surface
δ	initial propellant thickness

Number mean pit diameter is defined as midpoint on diameter—number-percent-distribution curve.

Pit density is the number of pits per unit area.

APPARATUS AND PROPELLANTS

Centrifuge

The centrifuge at the Langley Research Center was previously used as described in reference 11. It was modified for this study to increase the rotational radius to the propellant surface from 1.14 to 2.03 m (45 to 80 in.). A photograph of the modified centrifuge with a test motor mounted on each arm is shown in figure 1. The motor shown on the right side of the photograph includes the extinction apparatus which is described in a later section. The test motor was mounted on the centrifuge in a manner that eliminated rotational speed changes due to motor thrust. The increase in acceleration due to regression of the 5.08-cm-thick (2.0 in.) propellant web from an initial radius of 2.03 m (80 in.) was 2.5 percent. The rotational speed of the centrifuge was measured with a 60 pulse/revolution tachometer and a pulse counter. The centrifuge was brought to the desired speed before the rocket test motor was ignited.

Test Motor

The unidirectional-burning slab motor shown in figure 2 was utilized to minimize the effects of propellant grain geometry and spin-induced vortex flow so that the transient burning rate could be investigated in a nearly uniform acceleration environment. The lower insert on which the propellant slab was bonded and the upper insert that formed the top of the rectangular gas port were within the cylindrical pressure vessel. All propellant slabs used in the motor were 6.9 cm (2.7 in.) wide by 13.7 cm (5.4 in.) long. A steel spacer plate was used under thinner slabs <5.08 cm (<2.0 in.) to maintain the propellant

surface in the same location with respect to the igniter gas ports as the web thickness was reduced in 1.27-cm (0.5 in.) increments.

Two ports were machined in the head-end plate to provide for chamber pressure measurements. Strain-gage pressure transducers were connected to the pressure ports with 0.64-cm (1/4 in.) stainless-steel tubing. Various nozzle throat diameters were used to obtain the desired high, medium, and low pressure levels.

Extinction Test Apparatus

A blowoff nozzle and water quench system were employed so that the propellant could be partially burned while spinning, then extinquished, and examined for surface geometry changes. The test motor nozzle assembly was modified to accept two 0.64-cm-diameter (0.25 in.) explosive bolts for release of a plate holding the graphite nozzle insert. When the explosive bolts were activated during motor burning, the motor throat area was rapidly increased and a solenoid valve released a small amount of water into the chamber through the modified head-end plate and upper insert. The water cooled the chamber and prevented reignition. These modifications to the test motor are not shown in figure 2 for the sake of clarity.

Propellant

Three batches of aluminized polybutadiene acrylic acid (PBAA) propellant were used during the investigation. The propellant formulation and physical properties are given in table I. The static burning-rate data from the three propellant batches were least-squares fitted to the equation $r = a(p/p_{ref})^n$. The calculated burning-rate constant a was 7.80 mm/sec (0.307 in./sec) and the pressure exponent n was 0.255 when p_{ref} was 3.45 MN/m^2 (500 psia). The reproducibility of these data indicated that batch-to-batch variations in burning rate should not have affected the test results.

PROCEDURE

Test Procedure

The motors were fired at the test cell ambient temperature which was maintained at $21^O \pm 3^O$ C ($70^O \pm 5^O$ F). After motor burnout, the centrifuge was gradually stopped. Each test motor was disassembled and the lower insert and the nozzle were examined. Any remaining metallic residue from the lower insert was collected in a plastic bag and placed in a desiccator until analysis could be performed.

Since the magnitude of the burning-rate increase due to the imposed acceleration was unknown, the nozzle throat diameter required to give the desired average operating pressures could not be determined until a preliminary burning-rate—acceleration rela-

tionship had been defined. In order that tests could be conducted at nominal average chamber pressures of 2.07, 4.14, 6.21, and 8.27 MN/m^2 (300, 600, 900, and 1200 psia), high and low pressure tests were first conducted at each of the seven normal acceleration levels from 0g to 140g (1g = 9.8 m/sec^2) in 20g increments with the nozzle throat diameters sized from the K-p curve obtained from static tests. (The K-p curve is a plot of the ratio of the burning surface area to the nozzle throat area as a function of the average chamber pressure.) The static curve was established by using estimated nozzle throat sizes. These initial tests were used to generate a K-p curve for each acceleration level, from which the throat diameters for the desired pressure levels could then be calculated.

Variable web thickness tests were conducted at the medium pressure for each acceleration. The initial portion of the pressure histories with variable propellant web thicknesses was reproduced, even though the average pressure changed because of the dependence of burning rate on propellant distance burned under acceleration conditions.

The extinction tests were conducted in a manner similar to the other acceleration tests, except that, at a preprogramed time during motor burning, the explosive bolts and the water control solenoid were electrically activated.

Data Reduction

Since there was no available means of measuring instantaneous propellant burning rate, the instantaneous burning rate r_t was calculated from the pressure time history and motor characteristics by equating the mass flow from the burning surface to the nozzle discharge obtained from the average discharge coefficient for a given test. The equation

$$r_t = \frac{A_t \delta p_t}{\int_{t_i}^{t_b} A_t p_t \, dt} \tag{1}$$

was employed to include the effects of nozzle erosion. Nozzle erosion was assumed to be exponential; therefore, the throat area A_t was defined as

$$A_t = \frac{\pi}{4} d_{t,i}^2 + \frac{\pi}{4}\left(d_{t,f}^2 - d_{t,i}^2\right)\frac{t}{t_b} \exp\left(\frac{t}{t_b} - 1\right) \tag{2}$$

where $d_{t,i}$ and $d_{t,f}$ were the initial and final throat diameters, respectively.

6

The propellant distance burned to time t was calculated by integrating equation (1) to obtain

$$DB = \frac{\delta \int_{t_i}^{t} A_t p_t \, dt}{\int_{t_i}^{t_b} A_t p_t \, dt} \tag{3}$$

The test motor performance characteristics based on pressure burn time were calculated and listed; then the instantaneous pressure, instantaneous burning rate, and distance burned were calculated and tabulated at 0.040-sec intervals. The instantaneous chamber pressure and rate data were then plotted (for each acceleration level) with distance burned as a parameter. Thus, the burning rate could be interpolated for fixed values of acceleration, pressure, and distance burned. An example of the instantaneous rates is shown in figure 3 for the 140g acceleration level. The instantaneous rates at ignition and burnout were not used because of the highly transient nature of these processes.

The burning rates shown in figure 3 are typical data. The complete data tabulation is shown in table II. (The r_t data from a single motor firing are shown as solid symbols in fig. 3.) The lines represent the least-squares fit of the data. Values of a and n for all experimentally determined burning rates are given in table III for p_{ref} = 3.45 MN/m^2 (500 psia). These correlations were then used to obtain values of burning rate and distance burned for the nominal average pressure values. The curves presented in the remainder of this report are based on these values.

The accuracy of calculated r_t was spot checked by comparing the average rate computed from the calculated instantaneous data with $\bar{r}$ based on pressure burn time and measured web thickness. There was less than 0.5 percent difference in the rates of all points randomly checked. Because of the care taken to accurately measure the parameters used to calculate r_t, the r_t data should be accurate to ±2 percent.

Residue Analysis

The metallic residue that was retained on the lower insert of the burned-out motors by the acceleration force was carefully collected. The residue was analyzed to determine the general shape of the particles. Before the analysis the particles were washed with methyl ethyl ketone on a 100-mesh screen to separate the carbonaceous material resulting from the liner char from the metallic Al/Al_2O_3 residue. The characteristic shape of the particles retained on each sieve was identified along with the weight retained. The shapes were categorized as spheres, buttons, irregular agglomerates, and sheets. In order to

determine the transient-residue characteristics, motors were tested with propellant web thicknesses of 1.27, 2.54, and 3.81 cm (0.5, 1.0, and 1.5 in.) in addition to the 5.08-cm (2.0 in.) web used for the burning-rate data. The residue collection tests were conducted with the nozzle throat diameters used for the medium pressure 4.14-MN/m^2 (600 psia) 5.08-cm (2.0 in.) web tests. Two firings were conducted at each web thickness and at each of the test accelerations. Additional tests were conducted at 140g to determine the effect of pressure on the residue remaining from the 5.08-cm (2.0 in.) web motor. It was realized that the residue remaining at motor burnout may differ from that retained on the burning propellant surface. (See ref. 8.) However, the change in the residue characteristics with distance burned and acceleration was an available means of investigating the complex combustion phenomena associated with acceleration-induced transient burning-rate augmentation of the aluminized propellant. The specific residue weight was defined as the total residue weight divided by the propellant burning surface area.

Extinction Test Analysis

Photographs of the pitted propellant surface were made and the pit diameters and number density of 25.8 cm^2 (4.0 in^2) of the propellant surface were measured from the photographs by use of a Zeiss TGZ-3 Particle-Size Analyzer. The diameters reported are approximate because the exact edge of the pit was not always well defined in the photographs. The number mean pit diameters are reported at a given test condition. Number mean pit diameter is defined as the midpoint on a diameter—number-percent-distribution curve.

DISCUSSION OF RESULTS

Tests were conducted to determine the effects of normal acceleration into the propellant on the burning-rate augmentation, on the retention of metallic residue, and on the condition of the propellant surface following extinction. The results from these three areas are presented followed by "Correlation of Results." The transient burning-rate data were analyzed as a function of propellant distance burned rather than burning time. This procedure facilitated correlation of the residue data from motor firings having variable propellant web thicknesses with the transient-burning rate data.

Burning Rate

Typical pressure histories for motors that had nozzles sized for average chamber pressures of 4.14 MN/m^2 (600 psia) are shown in figure 4 for several accelerations. These traces cannot be compared directly since the throat area was changed to maintain the average pressure as the acceleration level was increased.

The 5.08-cm (2.0 in.) web motors were tested at each acceleration level from 0g to 140g normal acceleration in 20g increments to determine the rate augmentation. The average burning-rate augmentation $(r/r_0)_{av}$ based on t_b and the maximum rate augmentation $(r/r_0)_{max}$ (the maximum instantaneous rate divided by static rate) at 3.45 MN/m^2 (500 psia) were plotted as a function of acceleration level in figure 5. The largest change in rate augmentation occurred at lower accelerations between 20g and 60g. The decreased sensitivity of the average rate augmentation indicates a saturation of the mechanism causing the burning-rate augmentation with increasing acceleration level. Similar results were previously observed in 1.27-cm (0.5 in.) web test motors with a similar propellant (ref. 11).

The instantaneous burning rates r_t, calculated as discussed in the procedures, are shown in figure 6. The r_t data at DB = 2.54 mm (0.10 in.) and zero normal acceleration were used as the initial burning rates for the acceleration tests. This procedure eliminated ignition transient effects by assuming that for small distances burned, the burning rate under acceleration was equal to the static rate. The symbols with ticks in figures 6(b) to 6(h) at DB = 50.8 mm (2.0 in.) are the static r_t data at DB = 48.3 mm (1.9 in.) from figure 6(a). These data points were included as reference points to indicate the increased rate due to the acceleration environment. The unidirectional-burning slab motor was designed to give neutral burning pressure time histories. However, the rates shown in figure 6(a) for the static or nonspin tests indicate a slight increase in calculated burning rate r_t of 8 percent with increasing DB. This variation did not adversely affect the conclusions, since the acceleration-induced rates were much larger than this variation.

At accelerations of 20g and 40g (figs. 6(b) and 6(c)) the instantaneous burning rates r_t increased with increasing distance burned. When the acceleration was increased to 60g and 80g (figs. 6(d) and 6(e)), r_t increased, passed through a maximum, and then continued to decrease until motor burnout. At accelerations of 100g to 140g (figs. 6(f), 6(g), and 6(h)), r_t increased to a maximum, decreased, and then leveled off somewhat as DB increased. At accelerations of 40g, 60g, and 80g the 5.08-cm (2.0 in.) web was not sufficient to permit achievement of the quasi-equilibrium rate observed at the higher accelerations.

Figure 7 shows a composite of the curves for r_t plotted against DB at 4.14 MN/m^2 (600 psia) which allows comparison of the changes in transient burning rate with increasing acceleration level at this pressure.

The maximum rate and the distance burned to achieve $r_{t,max}$ are shown in figures 8 and 9, respectively, as a function of acceleration with pressure as a parameter. Figure 8 shows that $r_{t,max}$ increased with increasing acceleration up to 100g. Figure 9 illustrates the decreasing distance burned to achieve $r_{t,max}$ with increasing accelera-

tion. At 20g, $r_{t,max}$ occurred near motor burnout, whereas at 140g it occurred much earlier, DB = 15.24 mm (0.60 in.). The distance burned to $r_{t,max}$ showed no strong dependence on pressure, except at the 60g acceleration level.

Figure 10 shows the variation in r_t at a distance burned of 48.3 mm (1.9 in.) as a function of normal acceleration with pressure as a parameter. The curves were drawn through the data points that indicated quasi-equilibrium burning rates with respect to DB. The data points with arrows indicate that r_t had gone through a maximum, was decreasing, but had not reached a constant rate at motor burnout.

In the quasi-equilibrium region, r_t is essentially independent of distance burned. Thus it may be possible to use the curves in figure 10 to predict the quasi-equilibrium burning rate for values of distance burned beyond 48.3 mm (1.9 in.) at a given acceleration. If this prediction method could be shown to hold, one could, with confidence, use similar subscale data to predict the performance of operational motors with greater web thickness. The technique has the obvious advantage of avoiding the cost of extensive full-scale acceleration testing and should be explored more fully.

The acceleration-induced rate augmentation was dependent on chamber pressure as shown parametrically in figure 6. Typical data indicating the increased burning-rate augmentation with increased chamber pressure are shown in figure 11 for the 140g acceleration level. At 2.07 MN/m^2 (300 psia) the maximum burning-rate augmentation was 1.23. The burning-rate augmentation increased to 1.42 when the pressure was increased to 8.27 MN/m^2 (1200 psia). It was concluded that increased burning-rate augmentation with increased pressure resulted from improved aluminum combustion efficiency at the higher pressure level as evidenced by a decrease in the weight of metallic residue retained (to be presented in a later section).

Residue Analysis

Results from earlier extinction tests (ref. 11) of partially burned 1.27-cm (0.5 in.) web motors indicated the presence of metallic residue in pits formed on the propellant surface. It was concluded that the presence of the metallic residue was one cause of the average burning-rate augmentation observed.

During the subject investigation, the metallic residue retained on the lower inserts of the burned-out motors by the centrifugal acceleration force was collected and analyzed for correlation with the acceleration-induced burning-rate augmentation. Figure 12 illustrates the variation of total residue weight W and specific residue weight w as a function of propellant web thickness for various accelerations. The results of the residue classification are indicated at the top of each figure as weight percent of the indicated geometry. The percentages encircled denote the classification of the majority of the residue at a given web thickness.

10

The changes in residue characteristics with distance burned indicate the transient nature of the residue growth process at a given acceleration. For the lower accelerations the majority of residue remained spherical as the web thickness increased to 5.08 cm (2.0 in.). At 80g, the residue was mostly spherical for webs of 2.54 cm (1.0 in.) or less, after which buttons and irregular particles formed with increased distance burned.

As the acceleration level was increased, sheets of residue formed. The percentage of sheeted residue at a given web thickness increased and the distance burned to produce the sheets was reduced with increased acceleration level. Thus, the data substantiated reference 7 data which suggested that the propellant surface becomes flooded when sufficient residue has been retained.

Figure 13 illustrates the variation in residue weight and characteristics for the 5.08-cm (2.0 in.) web motor tests as a function of normal acceleration. The residue weight increased exponentially with acceleration. At 140g, 1.71 percent of the nominal propellant slab weight was retained. As the acceleration level increased, the residue character progressed from spherical particles to sheets of residue covering the lower insert. Thus, the flooding of the burning surface with sheets of residue was a function of both acceleration and distance burned.

A composite semilogarithmic plot of the average residue weight and specific residue weight are shown in figure 14 as a function of distance burned. Figure 14 shows the nearly exponential growth in residue weight with increasing distance burned. The data indicate that the residue weight retention process can be described by the first-order kinetic equation

$$\frac{dW}{dDB} = AW \tag{4}$$

which represents a "collision" process where the growth rate dW/dDB depends on the amount of residue present. The growth constant A was not strongly acceleration dependent. The growth process is consistent with the collision reasoning as long as the residue does not cover the major fraction of the burning surface. Results from the extinction tests (discussed in the next section) indicated discrete pits at large values of DB in regions where the residue data indicated sheeting. The results of films taken of similar propellants (ref. 2) indicate discrete molten agglomerates retained on burning surface with a progression from spherical particles to shallow pools. Thus, the molten residue may retain its discrete particulate nature, with increasing particle diameter on or above the burning surface, and the sheeting result from agglomeration of these particles at motor burnout.

The average residue weight at DB = 50.8 mm (2.0 in.) is shown in the semilogarithmic plot of figure 15. This figure illustrates the exponential increase in residue weight with increasing acceleration. An explanation of the exponential dependence of residue weight on normal acceleration was not attempted.

The effect of pressure on residue weight was examined by firing additional 5.08-cm (2.0 in.) web motors at elevated and reduced pressure levels at 140g. Figure 16 shows the results of these tests. Although there was scatter in the residue data, the weight retained decreased with increasing average motor pressure. The residue weight decreased by a factor of 2.5 as the pressure was increased from 1.04 to 7.59 MN/m^2 (150 to 1100 psia).

Extinction Tests

In order to gain better understanding of the effect of the retention of metallic residue on or above the burning propellant surface, the test motor was modified such that the propellant could be extinguished after burning for various times at selected acceleration levels. The propellant surface could then be examined for changes in pit characteristics.

Photographs of the resultant propellant surface from extinction tests conducted with the medium pressure nozzle at the time of peak pressure or largest burning rate are shown in figure 17 for normal accelerations of 0g, 40g, 60g, 80g, 100g, and 120g. The 140g photograph is shown as one of the series of photographs in figure 20. No figure is shown at 20g since its surface was similar to the smooth surface obtained from the 0g normal acceleration test.

Figure 17 shows that as the acceleration level was increased to 40g, the propellant surface became pitted. When the acceleration level was further increased, the pit diameter became limited by and decreased with increased pit density (number of pits per unit area).

The approximate number mean pit diameters and pit densities were measured and the results from the analysis are shown in figure 18. The photograph at 40g (fig. 17) showed both large and small pits. At 40g, the mean diameter for each of the distributions as well as the maximum diameter are shown to indicate the variation obtained. Above 80g the mean pit diameter decreased slightly with increasing acceleration level as shown in figure 18.

The increased number of pits and the decreased pit size with increasing acceleration at the peak burning rate indicate that the residue retained just above the burning surface caused localized increased burning rates in the vicinity of the residue particles. In some cases residue particles remained in their pits during extinction.

Figure 19 compares the pressure history from a 5.08-cm (2.0 in.) web test and the pressure histories resulting from the extinction tests with the same nozzle size at 140g. Extinction tests were conducted when the pressure was increasing, at a maximum, decreasing, and in the quasi-equilibrium region following the decline. The agreement in the pressure histories in the figure also illustrates that the transient burning-rate augmentation was very reproducible.

Figure 20 shows photographs of extinguished propellant surface as a function of selected calculated distance burned or burning time at 140g. The result of the 0g normal acceleration extinction test is also shown in figure 20 for comparison.

There was a gross change in the resultant propellant surface as a function of distance burned. The pit diameter increased, and the pit density decreased with increased distance burned. This drastic change in propellant surface indicated the transient effect of the metallic residue on the local burning rate.

The number mean pit diameter and pit density were plotted as a function of distance burned in figure 21. The pit diameter increased almost linearly with DB. The pit density decreased exponentially with increasing DB. This change in pit characteristics as a function of DB indicates that any proposed local burning-rate model should include the acceleration-induced transient burning-rate augmentation by including time or distance-dependent pitting characteristics.

Clayton T. Crowe of Washington State University has extended the United Technology Center (UTC) local heat feedback model to predict the reduction in r/r_0 as the spherical residue particles grow to become more platelet shaped. The model is in agreement with the limited data available. The UTC model also predicts the observed behavior of r/r_0 on n, p, and r_0. The lack of transient residue growth and accumulation models severely limits the prediction of r/r_0 using the current heat feedback models.

The relatively large mean pit diameters experienced indicate that caution should be exercised in the use of small strands to evaluate acceleration effects on solid-propellant burning rate since the area of a single pit can be on the order of the burning surface area.

Correlation of Results

The instantaneous burning-rate data and the residue data given in figures 6 and 12 were examined for correlation between the residue growth process and the acceleration-induced transient burning-rate augmentation. Two acceleration levels were chosen for presentation, although the discussion herein was found to apply at all acceleration levels. The 80g and 140g data were selected because these data were typical of the two types of instantaneous rate data observed, that is, at 80g the burning rate increased, gradually reached a maximum at DB = 25.4 mm (1.0 in.), and continued to decrease until motor

burnout; at 140g the burning rate increased rapidly, reached a maximum at DB = 15.2 mm (0.6 in.), decreased, and then continued at a quasi-equilibrium rate independent of DB.

The instantaneous burning rate at 4.14 MN/m^2 (600 psia), the residue weight, and the residue shape characteristics are shown in figure 22 for the 80g and 140g acceleration levels as a function of distance burned. In all cases the point of maximum burning rate corresponded to a distance burned where the majority of the residue particles were spherical. The burning rate was observed to have passed through the maximum and to be decreasing when the residue analysis indicated that the spherical particles had progressed to buttons. The quasi-equilibrium rate coincided with the formation of sheeted residue. Although the residue weight increased exponentially with distance burned, only a portion of the total residue was associated with the maximum burning-rate augmentation (fig. 22) except at the lower acceleration where the maximum r_t occurred near burnout. These data and the photographs from the extinction tests indicate that the transient burning-rate augmentation results from local burning-rate increases controlled by the residue particle characteristics and number density rather than total residue weight. Thus the growth characteristics of the residue, as aluminum becomes available at the receding surface, correlates the acceleration-induced transient burning-rate augmentation.

CONCLUDING REMARKS

The acceleration-induced transient burning-rate augmentation of a polybutadiene acrylic acid (PBAA) propellant containing 16 weight percent of aluminum was characterized at 2.07 to 8.27 MN/m^2 (300 to 1200 psia) with nearly constant centrifugal accelerations from 0g to 140g normal into the burning surface. Instantaneous burning-rate data were calculated from the pressure histories of a test motor with 96.77 cm^2 (15 in^2) of burning area and a 5.08-cm-thick (2.0 in.) propellant web. Additional acceleration tests were conducted with reduced propellant web thicknesses of 3.81, 2.54, and 1.27 cm (1.5, 1.0, and 0.5 in.). The metallic residue collected from the various web thickness tests was characterized by weight and shape and correlated with the instantaneous burning-rate measurements. Rapid-depressurization extinction tests were conducted in order that surface pitting characteristics due to localized increased burning rate could be correlated with the residue analysis and the instantaneous burning-rate data.

The acceleration-induced burning-rate augmentation was strongly dependent on propellant distance burned, or burning time, and thus was transient in nature. The results from the extinction tests and the residue analyses indicate that the transient rate augmentation was highly dependent on local enhancement of the combustion zone heat feedback to the surface by the growth of molten residue particles on or just above the burning

surface. The size, shape, and number density of molten residue particles, rather than the total residue weight, determined the acceleration-induced burning-rate augmentation.

Langley Research Center,
  National Aeronautics and Space Administration,
    Hampton, Va., February 14, 1972.

REFERENCES

1. Manda, Leo J.: Compilation of Rocket Spin Data. Vol. II: Literature Survey. Rep. No. 3001-2 (Contract No. NAS1-6833), Electron. & Space Div., Emerson Elec. Co., July 22, 1968. (Available as NASA CR-66641.)

2. Willoughby, P. G.; Baker, K. L.; and Hermsen, R. W.: Photographic Study of Solid Propellants Burning in an Acceleration Environment. Contract No. NAS1-8796, United Technol. Center. (Available as NASA CR-66824.)

3. Willoughby, Paul G.; Crowe, Clayton T.; Dunlap, Roger; and Baker, K. L.: Investigation of Internal Ballistic Effects in Spinning Solid Propellant Motors. UTC 2281-FR (Contract No. N00017-67-C-2429), United Technol. Center, Oct. 1968. (Available from DDC as AD 847 282.)

4. Burchard, J. K.; Hermsen, R. W.; Dunlap, R.; Lee, J. T.; and Willoughby, P. G.: Investigation of Performance Losses and Ballistics Effects in Solid Propellant Rockets. UTC 2197-FR (Contract No. NOw 66-0444-c), United Technol. Center, Apr. 14, 1967. (Available from DDC as AD 815 115.)

5. Crowe, C. T.; Willoughby, P. G.; Dunlap, R.; and Hermsen, R. W.: Investigation of Particle Growth and Ballistic Effects on Solid Propellant Rockets. UTC 2128-FR (Contract No. NOw 65-0222-f), United Technol. Center, June 15, 1966. (Available from DDC as AD 486 262.)

6. Bulman, M. J., and Netzer, D. W.: Burning Rate Acceleration Sensitivity of Double-Base Propellant. AIAA J., vol. 8, no. 6, June 1970, pp. 1155-1156.

7. Sturm, E. J.; and Reichenbach, R. E.: Aluminized Composite Solid-Propellant Burning Rates in Acceleration Fields. AIAA J., vol. 7, no. 11, Nov. 1969, pp. 2087-2093.

8. Anderson, J. B.; and Reichenbach, R. E.: An Investigation of the Effect of Acceleration on the Burning Rate of Composite Propellants. AIAA J., vol. 6, no. 2, Feb. 1968, pp. 271-277.

9. King, M. K.; and McHale, E. T.: An Optical Bomb Study of the Combustion of Solid Propellants in High Acceleration Fields. Contract No. N00014-67-C-0455, Atlantic Res. Corp., Mar. 1970. (Available from DDC as AD 508 083.)

10. Northam, G. B.; and Lucy, M. H.: Effects of Acceleration Upon Solid-Rocket Performance. J. Spacecraft Rockets, vol. 6, no. 4, Apr. 1969, pp. 456-459.

11. Northam, G. Burton: Effects of Steady-State Acceleration on Combustion Characteristics of an Aluminized Composite Solid Propellant. NASA TN D-4914, 1968.

12. Northam, George Burton: An Experimental Investigation of the Effects of Acceleration on the Combustion Characteristics of an Aluminized Composite Solid Propellant. M.S. Thesis, Virginia Polytech. Inst., 1965.

13. Glick, Robert L.: An Analytical Study of the Effects of Radial Acceleration Upon the Combustion Mechanism of Solid Propellant. Rep. No. 42-66 (Contract NAS7-406), Thiokol Chem. Corp., Dec. 1966. (Available as NASA CR-66218.)

14. Whitesides, R. Harold, Jr.; and Hodge, B. Keith: Theoretical Study of the Ballistics and Heat Transfer in Spinning Solid Propellant Rocket Motors. U-68-20A (Contract No. NAS 1-7034), Thiokol Chem. Corp., Aug. 1968. (Available as NASA CR-66639.)

TABLE I.- PROPELLANT FORMULATION AND PHYSICAL PROPERTIES

Composition

Ingredients	Weight, percent	Comments
PBAA binder	14	Includes curing agent, Thiokol HA polymer
Oxidizer	70	
Coarse ammonium perchlorate	45.5	180 μm weight median diameter
Fine ammonium perchlorate	24.5	20 μm weight median diameter
Aluminum powder	16	7 μm weight median diameter; irregular shape

Physical properties at 240° C (70° F)

Batch no.	Batch size		Maximum stress		Strain at maximum stress, percent
	kg	lb	MN/m^2	psi	
1	191	400	0.876	127	27
2	91	200	.876	127	28
3	191	400	1.034	150	26

Static burning rate

$$r = a\left(p/p_{ref}\right)^n$$

a = 7.80 mm/sec (0.307 in./sec)

n = 0.255

p_{ref} = 3.45 MN/m^2 (500 psia)

TABLE II.- BURNING-RATE DATA

(a) SI Units

Pressures and burning rates for distance burned of —

Accel., g units	2.54 mm		5.08 mm		10.16 mm		15.24 mm		20.32 mm		25.40 mm		30.48 mm		35.56 mm		40.64 mm		45.72 mm		48.26 mm		p̄	r̄
	p, MN/m²	r, mm/sec	p, MN/m²	r, mm/sec	p, MN/m²	r, mm/sec	p, MN/m²	r, mm/sec	p, MN/m²	r, mm/sec	p, MN/m²	r, mm/sec	p, MN/m²	r, mm/sec	p, MN/m²	r, mm/sec	p, MN/m²	r, mm/sec	p, MN/m²	r, mm/sec	p, MN/m²	r, mm/sec	MN/m²	mm/sec
0	2.544	7.06	2.551	7.06	2.579	7.19	2.634	7.34	2.634	7.38	2.620	7.37	2.599	7.37	2.572	7.32	2.544	7.29	2.503	7.21	2.461	7.14	2.572	7.26
	5.964	8.84	5.771	8.56	5.881	8.74	6.033	8.97	6.129	9.12	6.157	9.17	6.095	9.09	6.047	9.07	5.985	8.99	5.957	8.97	5.881	8.86	5.971	8.92
	4.054	8.03	4.171	8.28	4.240	8.43	4.199	8.36	4.185	8.36	4.151	8.33	4.082	8.20	3.971	8.03	3.854	7.85	3.730	7.65	3.654	7.52	4.027	8.10
	3.992	7.54	4.040	7.65	4.144	7.85	4.240	8.05	4.323	8.23	4.392	8.38	4.371	8.38	4.364	8.38	4.330	8.36	4.289	8.33	4.226	8.23	4.240	8.13
	5.585	8.05	5.709	8.23	5.929	8.59	6.136	8.92	6.350	9.25	6.426	9.40	6.405	9.40	6.426	9.47	6.350	9.45	6.219	9.32	6.191	9.30	6.143	9.02
	1.889	6.10	1.896	6.12	1.958	6.32	2.006	6.53	2.055	6.68	2.089	6.81	2.124	6.96	2.117	6.96	2.137	7.06	2.186	7.24	2.193	7.32	2.062	6.73
20	2.013	6.05	2.055	6.20	2.206	6.65	2.282	6.91	2.330	7.06	2.365	7.19	2.344	7.14	2.365	7.24	2.372	7.29	2.392	7.39	2.392	7.39	2.282	6.99
	2.234	6.40	2.248	6.45	2.317	6.68	2.392	6.88	2.448	7.06	2.475	7.19	2.489	7.24	2.489	7.29	2.482	7.32	2.475	7.34	2.461	7.32	2.413	7.01
	3.847	7.59	3.944	7.80	4.061	8.08	4.164	8.33	4.178	8.41	4.158	8.41	4.095	8.36	4.047	8.36	3.985	8.31	3.875	8.20	3.820	8.15	4.006	8.15
	3.847	7.82	3.916	7.95	4.006	8.15	4.102	8.38	4.171	8.56	4.213	8.69	4.233	8.76	4.220	8.76	4.199	8.76	4.151	8.71	4.123	8.71	4.095	8.43
	5.895	8.81	5.985	8.97	6.136	9.25	6.274	9.50	6.357	9.65	6.357	9.73	6.343	9.78	6.309	9.80	6.281	9.86	6.191	9.80	6.164	9.83	6.184	9.50
	6.605	8.56	6.681	9.45	6.812	9.65	6.984	9.93	7.074	10.13	7.074	10.19	6.971	10.13	6.950	10.16	6.853	10.13	6.778	10.13	6.681	10.06	6.840	9.93
40	2.227	7.04	2.303	7.26	2.358	7.44	2.303	7.29	2.275	7.21	2.282	7.26	2.248	7.16	2.255	7.21	2.248	7.19	2.220	7.16	2.213	7.14	2.261	7.21
	2.351	6.48	2.365	6.55	2.468	6.86	2.530	7.06	2.592	7.26	2.613	7.39	2.661	7.57	2.661	7.65	2.689	7.80	2.689	7.90	2.689	7.95	2.599	7.29
	3.461	7.32	3.503	7.44	3.654	7.80	3.792	7.65	3.923	8.48	4.068	8.84	4.220	9.25	4.226	9.35	4.226	9.42	4.109	9.27	4.033	9.17	3.916	8.56
	3.523	7.70	3.571	7.80	3.675	8.05	3.778	8.28	3.882	8.64	4.006	8.81	4.089	9.02	4.178	9.25	4.247	9.42	4.240	9.45	4.006	8.97	3.916	8.64
	5.536	8.94	5.736	9.27	5.709	9.27	5.826	9.50	6.081	9.98	6.378	10.54	6.584	10.95	6.688	11.20	6.722	11.35	6.619	11.28	6.550	11.23	6.150	10.41
	6.343	8.74	6.640	9.19	7.143	9.98	7.929	11.20	8.570	12.22	8.846	12.75	8.887	12.95	8.756	12.93	8.501	12.75	8.156	12.45	7.977	12.29	7.860	11.38
60	1.951	6.17	1.951	6.17	2.062	6.55	2.165	6.91	2.268	7.26	2.365	7.62	2.434	7.90	2.482	8.08	2.489	8.15	2.455	8.10	2.441	8.10	2.261	7.34
	3.682	8.51	3.833	8.74	4.040	9.19	4.289	9.78	4.509	10.31	4.626	10.59	4.592	10.52	4.468	10.26	4.289	9.86	4.020	9.30	3.889	8.99	4.213	9.70
	3.744	8.15	3.799	8.31	3.964	8.66	4.109	9.02	4.337	9.55	4.530	10.03	4.592	10.21	4.530	10.11	4.357	9.78	4.130	9.35	4.020	9.14	4.185	9.27
	4.909	8.28	4.957	8.38	5.592	9.47	6.226	10.59	6.764	11.61	6.964	11.99	6.950	12.01	6.819	11.86	6.578	11.53	6.316	11.18	6.178	11.00	6.123	10.57
	6.881	9.98	6.950	10.11	7.653	11.20	8.536	12.57	8.908	13.18	8.929	13.31	8.680	13.06	8.329	12.65	7.977	12.24	7.474	11.63	7.205	11.30	7.881	11.81
80	2.441	6.93	2.482	7.06	2.641	7.54	2.799	8.00	2.930	8.41	2.972	8.56	2.882	8.36	2.820	8.08	2.648	7.77	2.517	7.44	2.413	7.19	2.689	7.77
	1.903	6.32	1.896	6.32	2.006	6.71	2.172	7.26	2.310	7.75	2.351	7.90	2.372	7.98	2.344	7.90	2.289	7.75	2.206	7.47	2.206	7.52	2.193	7.37
	3.765	8.08	3.896	8.38	4.316	9.30	4.682	10.13	4.902	10.64	4.854	10.59	4.647	10.19	4.323	9.53	3.999	8.89	3.737	8.36	3.640	8.20	4.247	9.30
	3.420	7.62	3.496	7.80	3.751	8.38	4.220	9.45	4.633	10.41	4.819	10.85	4.750	10.74	4.592	10.41	4.309	9.83	4.082	9.35	3.944	9.07	4.164	9.42
	5.109	8.71	5.481	9.35	6.516	11.13	7.171	12.27	7.122	12.22	7.033	12.09	6.915	11.91	6.619	11.43	6.350	11.02	6.088	10.62	5.985	10.44	6.371	10.97
	NO TABULAR DATA																						8.680	12.32
100	NO TABULAR DATA																						2.951	8.20
	1.813	6.20	1.868	6.45	2.117	7.26	2.268	7.80	2.344	8.08	2.324	8.03	2.241	7.77	2.151	7.47	2.103	7.34	2.082	7.32	2.075	7.32	2.137	7.42
	3.475	7.67	3.599	7.98	4.171	9.27	4.688	10.46	4.813	10.77	4.785	10.77	4.633	10.46	4.454	10.13	4.226	9.70	4.068	9.40	3.985	9.27	4.261	9.60
	3.813	8.31	3.964	8.64	4.640	10.11	5.116	11.15	5.219	11.38	5.026	11.00	4.771	10.44	4.399	9.65	4.109	9.04	3.923	8.66	3.840	8.48	4.426	9.70
	5.502	8.71	6.095	9.68	7.736	12.34	8.350	13.36	8.487	13.64	8.260	13.34	7.867	12.78	7.364	12.01	6.819	11.23	6.481	10.80	5.702	10.69	7.157	11.61
	6.764	9.42	7.950	11.10	10.080	14.15	10.742	15.14	10.756	15.24	10.315	14.71	9.694	13.92	8.949	12.95	8.232	12.04	7.832	11.61	7.612	11.38	8.818	12.50
120	2.006	6.71	2.103	7.04	2.324	7.77	2.461	8.26	2.448	8.23	2.324	7.82	2.220	7.49	2.141	7.26	2.082	7.09	2.048	7.01	2.020	6.93	2.206	7.44
	2.420	6.86	2.537	7.14	2.930	8.26	3.254	9.19	3.316	9.37	3.213	9.09	3.054	8.69	2.937	8.38	2.854	8.18	2.785	8.03	2.765	7.98	2.923	8.33
	3.468	7.87	3.861	8.79	4.530	10.31	4.819	10.97	4.792	10.97	4.557	10.44	4.254	9.78	3.889	9.02	3.730	8.71	3.682	8.64			4.137	9.55
	3.696	8.53	4.013	9.27	4.606	10.67	4.806	11.15	4.716	10.97	4.502	10.49	4.302	10.06	4.137	9.73	3.999	9.42	3.930	9.32	3.875	9.22	4.240	9.91
	6.557	9.93	8.046	12.22	8.991	13.67	9.287	14.12	9.005	13.77	8.446	12.98	7.839	12.09	7.426	11.53	7.088	11.07	6.957	10.97	6.895	10.92	7.736	11.91
	5.392	8.89	6.550	10.80	7.626	12.60	7.681	12.70	7.729	12.78	7.302	12.09	6.784	11.25	6.571	10.90	6.405	10.64	6.178	10.31	6.136	10.24	6.681	11.07
140	2.282	6.73	2.496	7.37	2.965	8.76	3.013	8.94	2.820	8.38	2.661	7.92	2.558	7.65	2.530	7.62	2.530	7.65	2.517	7.67	2.517	7.70	2.627	7.87
	2.130	6.73	2.330	7.39	2.723	8.64	2.758	8.79	2.627	8.38	2.441	7.82	2.344	7.54	2.324	7.49	2.289	7.44	2.275	7.47	2.324	7.65	2.413	7.77
	3.640	8.26	4.054	9.19	4.881	11.07	4.757	10.97	4.516	10.44	4.213	9.75	3.985	9.25	3.847	8.97	3.737	8.74	3.702	8.69	3.675	8.64	4.185	9.50
	3.337	7.70	3.792	8.74	4.578	10.57	4.757	10.97	4.516	10.44	4.213	9.75	3.985	9.25	3.847	8.97	3.737	8.74	3.702	8.69	3.675	8.64	3.992	9.27
	5.502	8.94	6.840	11.13	7.984	13.03	7.998	13.08	7.495	12.29	6.936	11.40	6.502	10.80	5.661	10.52	6.191	10.31	6.081	10.21	6.005	10.11	6.536	10.77
	6.674	9.37	8.267	11.61	10.163	14.33	10.535	14.86	10.315	14.58	9.687	12.73	8.970	12.75	8.405	12.01	8.177	11.73	7.770	11.23	7.688	11.13	8.660	12.34

19

TABLE II.- BURNING-RATE DATA – Concluded

(b) U.S. Customary Units

Pressure and burning rates for distance burned of –

Accel., g units	0.1 in.		0.2 in.		0.4 in.		0.6 in.		0.8 in.		1.0 in.		1.2 in.		1.4 in.		1.6 in.		1.8 in.		1.9 in.		$\bar{p}$,	$\bar{r}$,
	p, psia	r, in./sec	p, psia	r, in./sec	p, psia	r, in./sec	p, psia	r, in./sec	p, psia	r, in./sec	p, psia	r, in./sec	p, psia	r, in./sec	p, psia	r, in./sec	p, psia	r, in./sec	p, psia	r, in./sec	p, psia	r, in./sec	psia	in./sec
0	369	0.278	370	0.278	374	0.283	382	0.289	382	0.291	380	0.290	377	0.290	373	0.288	369	0.287	363	0.284	357	0.281	373	0.286
	865	.348	837	.337	853	.344	875	.353	889	.359	893	.361	884	.358	877	.357	868	.354	864	.353	853	.349	866	.351
	588	.316	605	.326	615	.332	609	.329	607	.329	602	.328	592	.323	576	.316	559	.309	541	.301	530	.296	584	.319
	579	.297	586	.301	601	.309	615	.317	627	.324	637	.330	634	.330	633	.330	628	.329	622	.328	613	.324	615	.320
	810	.317	828	.324	860	.338	890	.351	921	.364	932	.370	929	.370	932	.373	921	.372	902	.367	898	.366	891	.355
	274	.240	275	.241	284	.249	291	.257	298	.263	303	.268	308	.274	307	.274	310	.278	317	.285	318	.288	299	.265
20	292	0.238	298	0.244	320	0.262	331	0.272	338	0.278	343	0.283	340	0.281	343	0.285	344	0.287	347	0.291	347	0.291	331	0.275
	324	.252	326	.254	336	.263	347	.271	355	.278	359	.283	361	.285	361	.287	360	.288	359	.289	357	.288	350	.276
	558	.299	572	.307	589	.318	604	.328	606	.331	603	.331	594	.329	587	.329	578	.327	562	.323	554	.321	581	.321
	558	.308	568	.313	581	.321	595	.330	605	.337	611	.342	614	.345	612	.345	609	.345	602	.343	598	.343	594	.332
	855	.347	868	.353	890	.364	910	.374	922	.380	922	.383	920	.385	915	.386	911	.388	898	.386	894	.387	897	.374
	958	.337	969	.372	988	.380	1013	.391	1026	.399	1026	.401	1011	.399	1008	.400	994	.399	983	.399	969	.396	992	.391
40	323	0.277	334	0.286	342	0.293	334	0.287	330	0.284	331	0.286	326	0.282	327	0.284	326	0.283	322	0.282	321	0.281	328	0.284
	341	.255	343	.258	358	.270	367	.278	376	.286	379	.291	386	.298	386	.301	390	.307	390	.311	390	.313	377	.287
	502	.288	508	.293	530	.307	550	.301	569	.334	590	.348	612	.364	613	.368	613	.371	596	.365	585	.361	568	.337
	511	.303	518	.307	533	.317	548	.326	563	.340	581	.347	593	.355	606	.364	616	.371	615	.372	581	.353	568	.340
	803	.352	832	.365	828	.365	845	.374	882	.393	925	.415	955	.431	970	.441	975	.447	960	.444	950	.442	892	.410
	920	.344	963	.362	1036	.393	1150	.441	1243	.481	1283	.502	1289	.510	1270	.509	1233	.502	1183	.490	1157	.484	1140	.448
60	283	0.243	283	0.243	299	0.258	314	0.272	329	0.286	343	0.300	353	0.311	360	0.318	361	0.321	356	0.319	354	0.319	328	0.289
	534	.335	556	.344	586	.362	622	.385	654	.406	671	.417	666	.414	648	.404	622	.388	583	.366	564	.354	611	.382
	543	.321	551	.327	575	.341	596	.355	629	.376	657	.395	666	.402	657	.398	632	.385	599	.368	583	.360	607	.365
	712	.326	719	.330	811	.373	903	.417	981	.457	1010	.472	1008	.473	989	.467	954	.454	916	.440	896	.433	888	.416
	998	.393	1008	.398	1110	.441	1238	.495	1292	.519	1295	.524	1259	.514	1208	.498	1157	.482	1084	.458	1045	.445	1143	.465
80	354	0.273	360	0.278	383	0.297	406	0.315	425	0.331	431	0.337	418	0.329	409	0.323	384	0.306	365	0.293	350	0.283	390	0.306
	276	.249	275	.249	291	.264	315	.286	335	.305	341	.311	344	.314	340	.311	332	.305	320	.294	320	.296	318	.290
	546	.318	565	.330	626	.366	679	.399	711	.419	704	.417	674	.401	627	.375	580	.350	542	.329	528	.323	616	.366
	496	.300	507	.307	544	.330	612	.372	672	.410	699	.427	689	.423	666	.410	625	.387	592	.368	572	.357	604	.371
	741	.343	795	.368	945	.438	1040	.483	1033	.481	1020	.476	1020	.469	960	.450	921	.434	883	.418	868	.411	924	.432
								NO TABULAR DATA														=	1259	.485
100								NO TABULAR DATA														=	428	0.323
	263	0.244	271	0.254	307	0.286	329	0.307	340	0.318	337	0.316	325	0.306	312	0.294	305	0.289	302	0.288	301	0.288	310	0.292
	504	.302	522	.314	605	.365	680	.412	698	.424	694	.424	672	.412	646	.399	613	.382	590	.370	578	.365	618	.378
	553	.327	575	.340	673	.398	742	.439	757	.448	729	.433	692	.411	638	.380	596	.356	569	.341	557	.334	642	.382
	798	.343	884	.381	1122	.486	1211	.526	1231	.537	1198	.525	1141	.503	1068	.473	989	.442	940	.425	827	.421	1038	.457
	981	.371	1153	.437	1462	.557	1558	.596	1560	.600	1496	.579	1406	.548	1298	.510	1194	.474	1136	.457	1104	.448	1279	.492
120	291	0.264	305	0.277	337	0.306	357	0.325	355	0.324	337	0.308	322	0.295	311	0.286	302	0.279	297	0.276	293	0.273	320	0.293
	351	.270	368	.281	425	.325	472	.362	481	.369	466	.358	443	.342	426	.330	414	.322	404	.316	401	.314	424	.328
	503	.310	560	.346	657	.406	699	.433	695	.432	661	.411	617	.385	590	.370	564	.355	541	.343	534	.340	600	.376
	536	.336	582	.365	668	.420	697	.439	684	.432	653	.413	624	.396	600	.383	580	.371	570	.367	562	.363	615	.390
	951	.391	1167	.481	1304	.538	1344	.556	1306	.542	1225	.511	1137	.476	1077	.454	1028	.436	1009	.432	1000	.430	1122	.469
	782	.350	950	.425	1106	.496	1114	.500	1121	.503	1059	.476	984	.443	953	.429	929	.419	896	.406	890	.403	969	.436
140	331	0.265	362	0.290	430	0.345	437	0.352	409	0.330	386	0.312	371	0.301	367	0.300	367	0.301	365	0.302	365	0.303	381	0.310
	309	.265	338	.291	395	.340	400	.346	381	.330	354	.308	340	.297	337	.295	332	.293	330	.294	337	.301	350	.306
	528	.325	588	.362	699	.430	708	.436	671	.413	623	.386	594	.365	582	.358	575	.354	566	.348	578	.356	607	.374
	484	.303	550	.344	664	.416	690	.432	655	.411	611	.384	578	.364	558	.353	542	.344	537	.342	533	.340	579	.365
	798	.352	992	.438	1158	.513	1160	.515	1087	.484	1006	.449	949	.425	821	.414	898	.406	882	.402	871	.398	948	.424
	968	.369	1199	.457	1474	.564	1528	.585	1496	.574	1405	.501	1301	.502	1219	.473	1186	.462	1127	.442	1115	.438	1256	.486

TABLE III.- BURNING-RATE RESULTS

(a) SI Units

Accel., g units (a)	2.54 mm		5.08 mm		10.16 mm		15.24 mm		20.32 mm		25.40 mm		30.48 mm		35.56 mm		40.64 mm		45.72 mm		48.26 mm	
	a, mm/sec	n	a, mm/sec	n	a, mm/sec	n	a, mm/sec	n	a, mm/sec	n	a, mm/sec	n	a, mm/sec	n	a, mm/sec	n	a, mm/sec	n	a, mm/sec	n	a, mm/sec	n
0	7.42	0.275	7.44	0.272	7.59	0.273	7.72	0.270	7.82	0.275	b7.87	0.276	b7.90	0.261	b7.87	0.266	b7.87	0.257	b7.87	0.245	7.82	0.238
20	7.32	.309	7.47	.350	7.67	.332	7.85	.329	7.98	.327	8.05	.320	8.05	.322	8.10	.317	b8.13	.316	b8.15	.310	8.15	.312
40	7.54	.277	7.70	.297	7.90	.306	8.15	.308	8.23	.396	8.38	.415	8.48	.426	8.56	.426	b8.64	.424	b8.66	.415	8.61	.413
60	7.77	.359	7.82	.369	8.18	.393	8.51	.425	8.79	.431	9.02	.416	b9.14	.393	b9.17	.372	9.12	.354	8.97	.338	8.86	.328
80	7.72	.326	7.90	.366	8.38	.426	8.81	.440	9.12	.416	b9.22	.404	9.17	.394	9.02	.373	8.76	.366	8.53	.366	8.43	.360
100	7.70	.312	8.03	.367	8.81	.426	9.30	.423	b9.47	.414	9.42	.404	9.22	.397	8.97	.386	8.76	.364	8.64	.351	8.64	.357
120	7.92	.331	8.43	.420	9.12	.424	b9.50	.395	b9.53	.386	9.27	.379	8.99	.364	8.81	.359	8.66	.354	8.56	.352	8.53	.354
140	7.80	.302	8.48	.377	9.42	.390	b9.55	.391	9.25	.402	8.89	.360	8.66	.386	8.64	.377	8.53	.352	8.51	.330	8.56	.316

(b) U.S. Customary Units

Accel., g units (a)	0.1 in.		0.2 in.		0.4 in.		0.6 in.		0.8 in.		1.0 in.		1.2 in.		1.4 in.		1.6 in.		1.8 in.		1.9 in.	
	a, in./sec	n	a, in./sec	n	a, in./sec	n	a, in./sec	n	a, in./sec	n	a, in./sec	n	a, in./sec	n	a, in./sec	n	a, in./sec	n	a, in./sec	n	a, in./sec	n
0	0.292	0.275	0.293	0.272	0.299	0.273	0.304	0.270	0.308	0.275	b0.310	0.276	b0.311	0.261	b0.310	0.266	b0.310	0.257	b0.310	0.245	0.308	0.238
20	.288	.309	.294	.350	.302	.332	.309	.329	.314	.327	.317	.320	.317	.322	.319	.317	b.320	.316	b.321	.310	b.321	.312
40	.297	.277	.303	.297	.311	.306	.321	.308	.324	.396	.330	.415	.334	.426	.337	.426	b.340	.424	b.341	.415	.339	.413
60	.306	.359	.308	.369	.322	.393	.335	.425	.346	.431	.355	.416	b.360	.393	b.361	.372	.359	.354	.353	.338	.349	.328
80	.304	.326	.311	.366	.330	.426	.347	.440	.359	.416	b.363	.404	.361	.394	.355	.373	.345	.366	.336	.366	.332	.360
100	.303	.312	.316	.367	.347	.426	.366	.423	b.373	.414	.371	.404	.363	.397	.353	.386	.345	.364	.340	.351	.340	.357
120	.312	.331	.332	.420	.359	.424	b.374	.395	b.375	.386	.365	.379	.354	.364	.347	.359	.341	.354	.337	.352	.336	.354
140	.307	.302	.334	.377	.371	.390	b.376	.391	.364	.402	.350	.360	.341	.386	.340	.377	.336	.352	.335	.330	.337	.316

Both tables carry the column-group heading: Burning-rate constants and pressure exponents for distance burned of —

aNormal into burning surface.

bMaximum or near-maximum values.

L-72-131

Figure 1.- Centrifuge.

PRESSURE PORT
PRESSURE PORT RELIEF
UPPER INSERT
PELLET CHAMBER
GAS PORT
PORT FOR IGNITION SQUIB
IGNITION GAS PORT
NOZZLE ASSEMBLY
PROPELLANT
LOWER INSERT

SECTION-AA
MOTOR CASE

PROPELLANT CHARACTERISTICS

LENGTH - 5.38 in.(136.7mm)

WIDTH - 2.75 in.(69.9mm)

WEB - 2.00 in.(50.8mm)

WEIGHT - 1.896 lb (860 g)

5.38 in.
(136.7 mm)
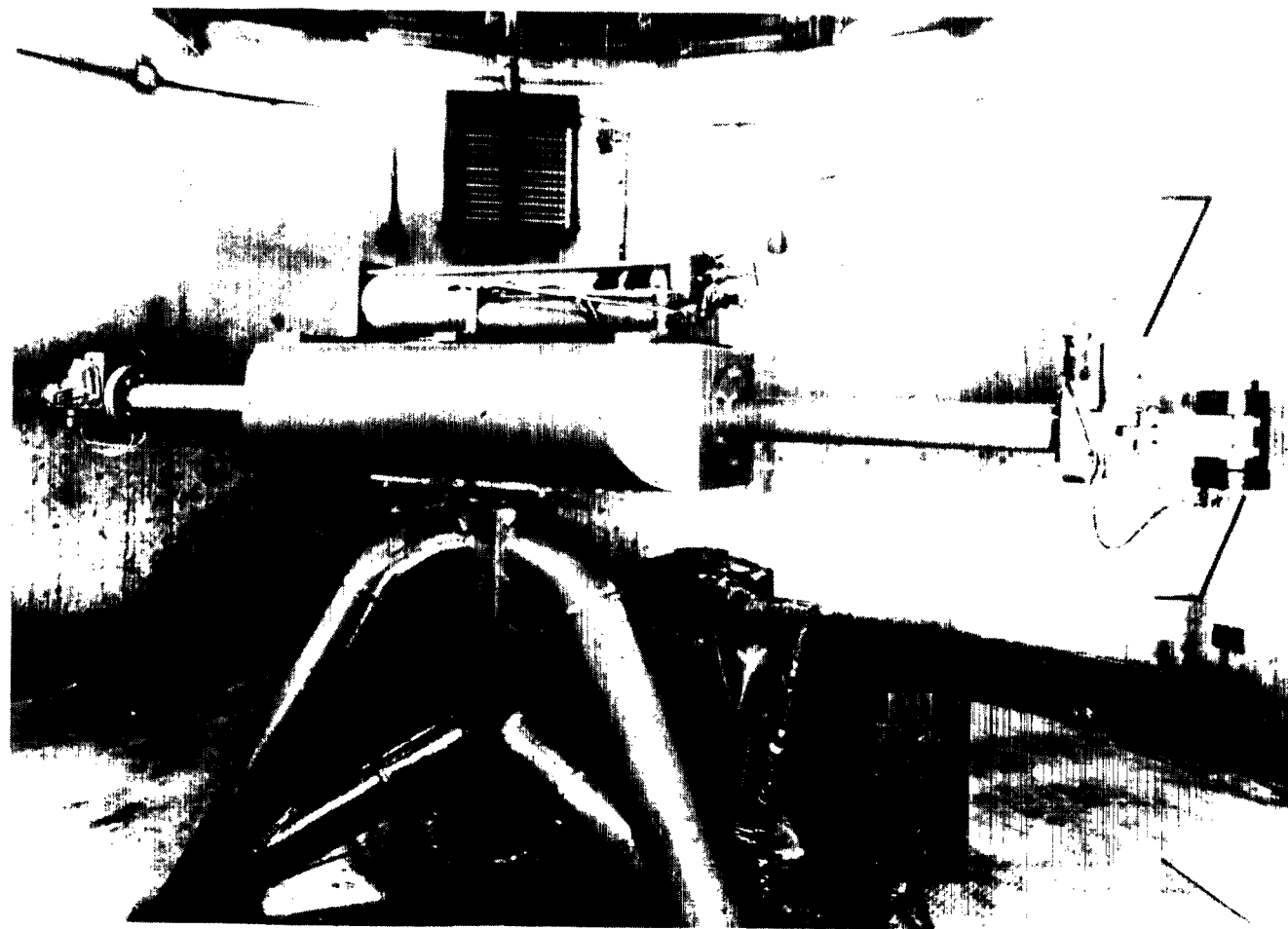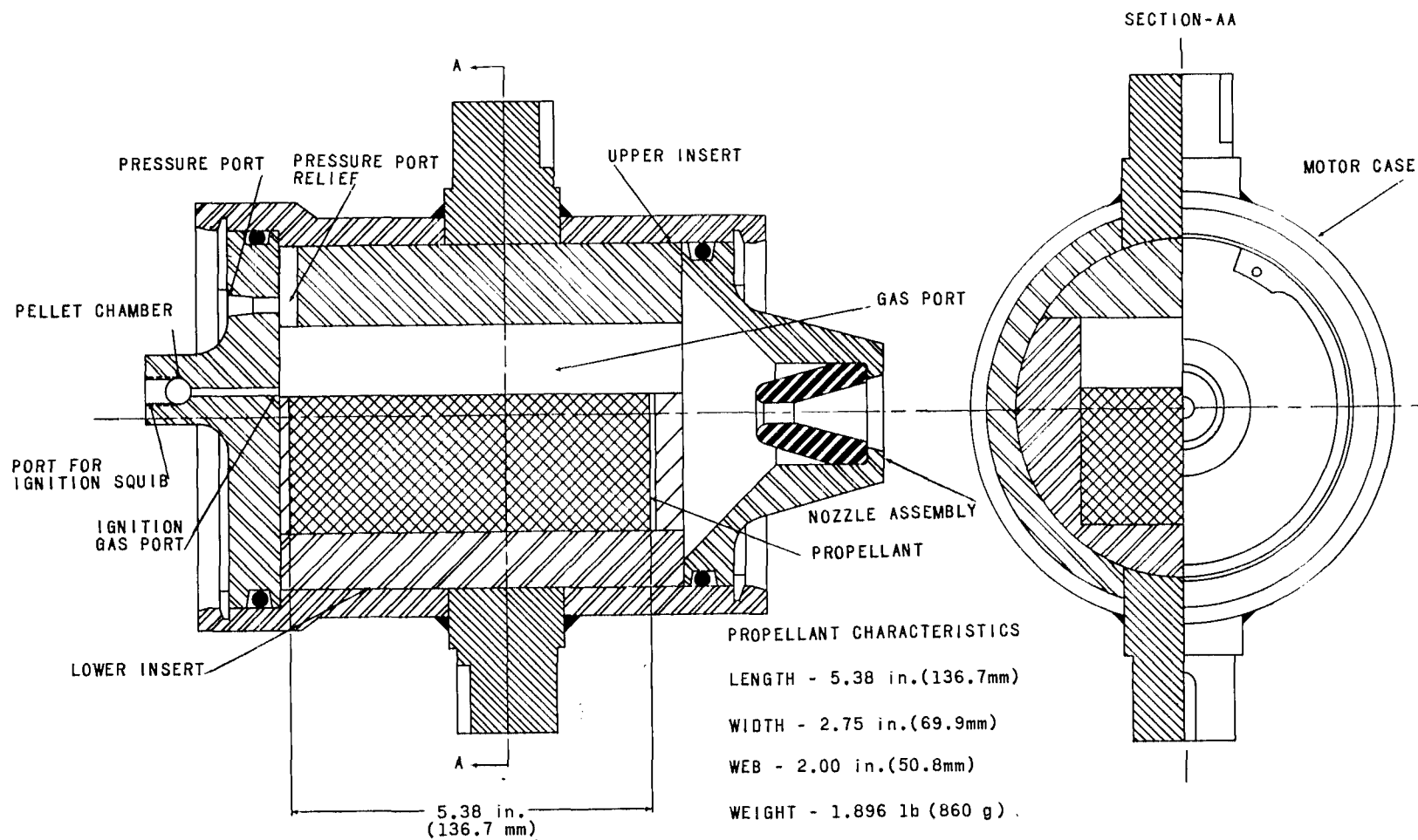
Figure 2.- Test motor.
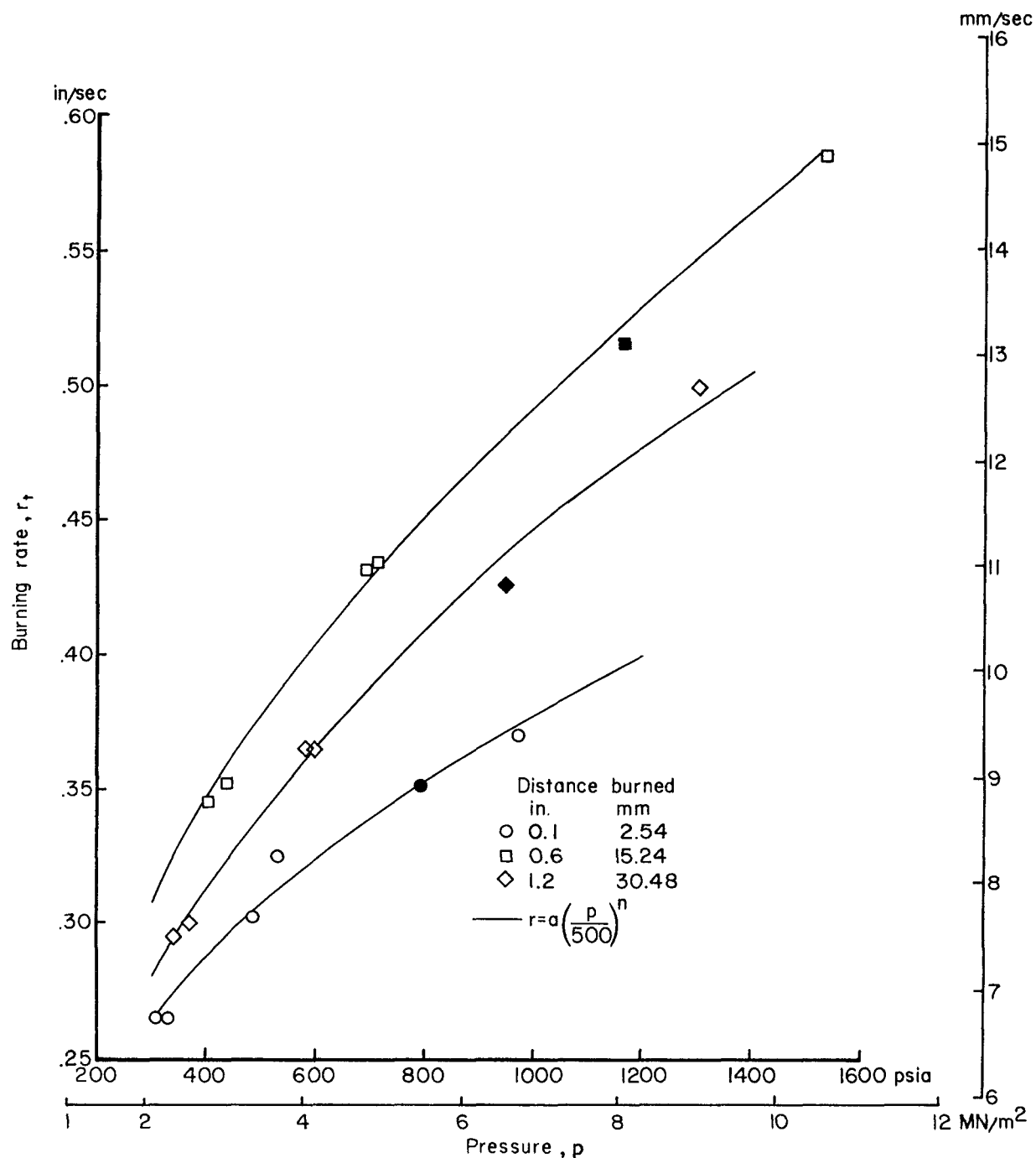
Figure 3.- Typical burning-rate data at 140g normal acceleration. Solid symbols
denote single test.

24
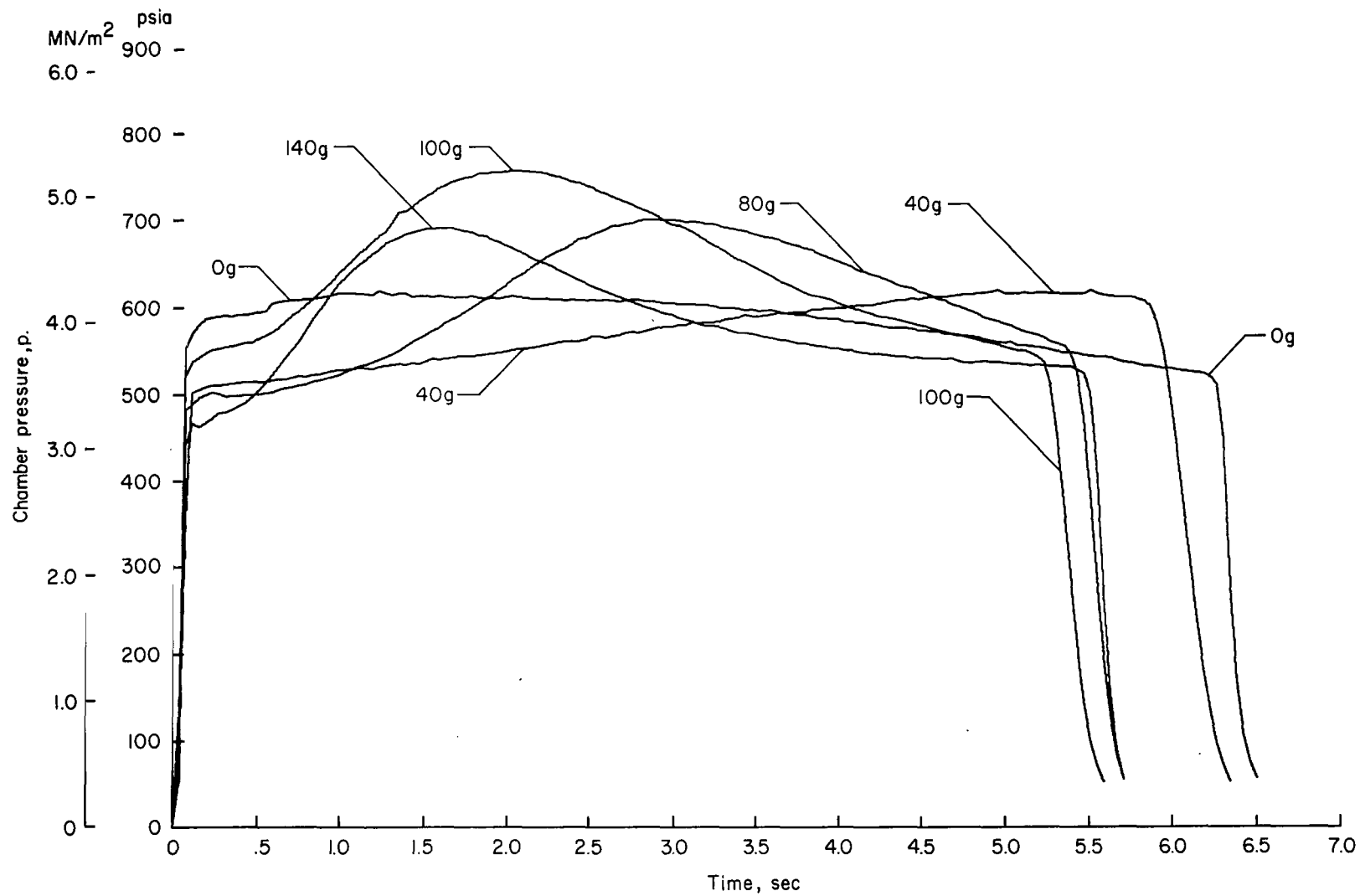
Figure 4.- Typical chamber pressure histories as a function of acceleration for 5.08-cm (2.0 in.) web motors.
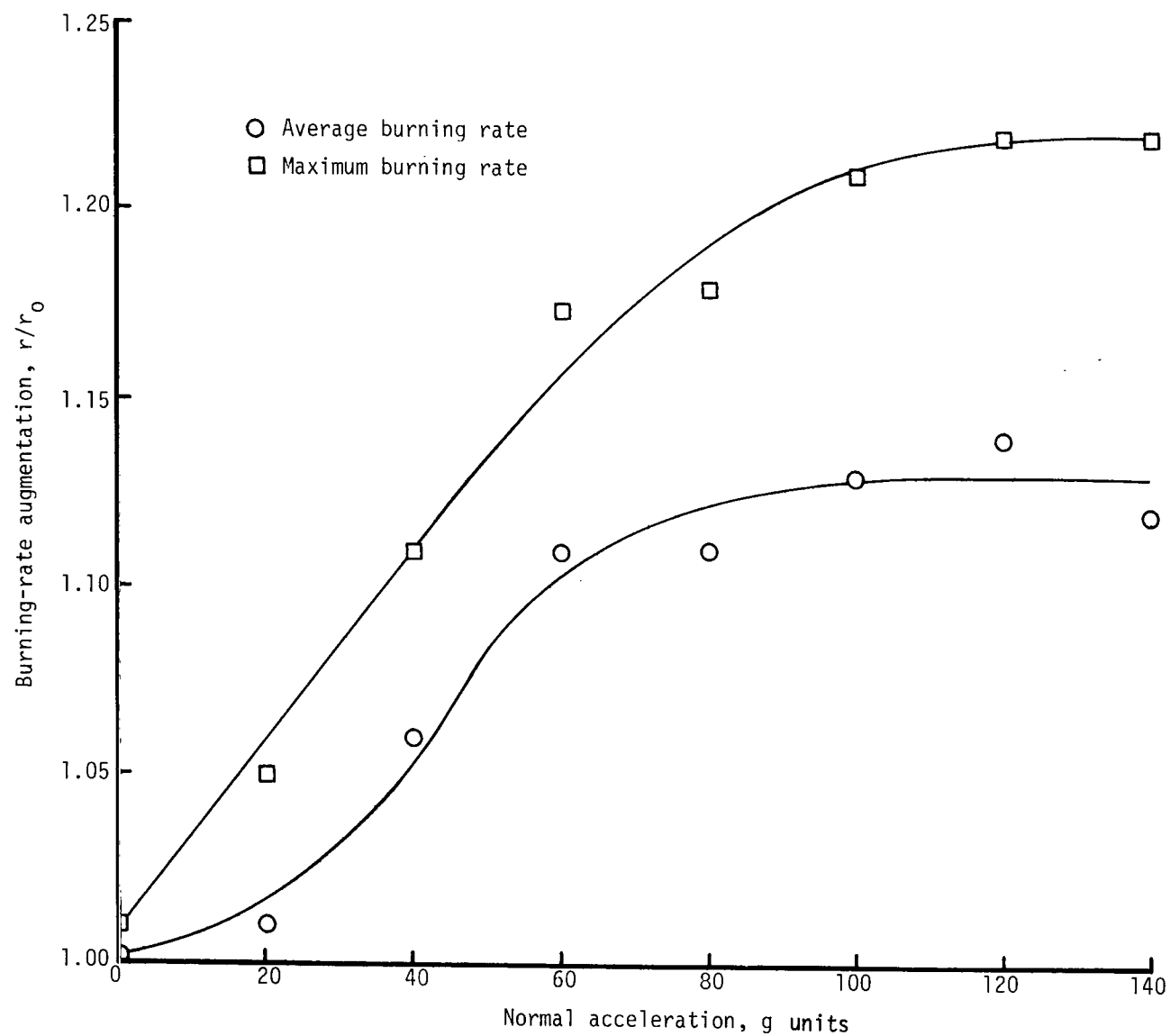
Figure 5.- Effect of acceleration on average and maximum burning-rate augmentation for 5.08-cm (2.0 in.) web motor. Pressure, 3.45 MN/m^2 (500 psia).
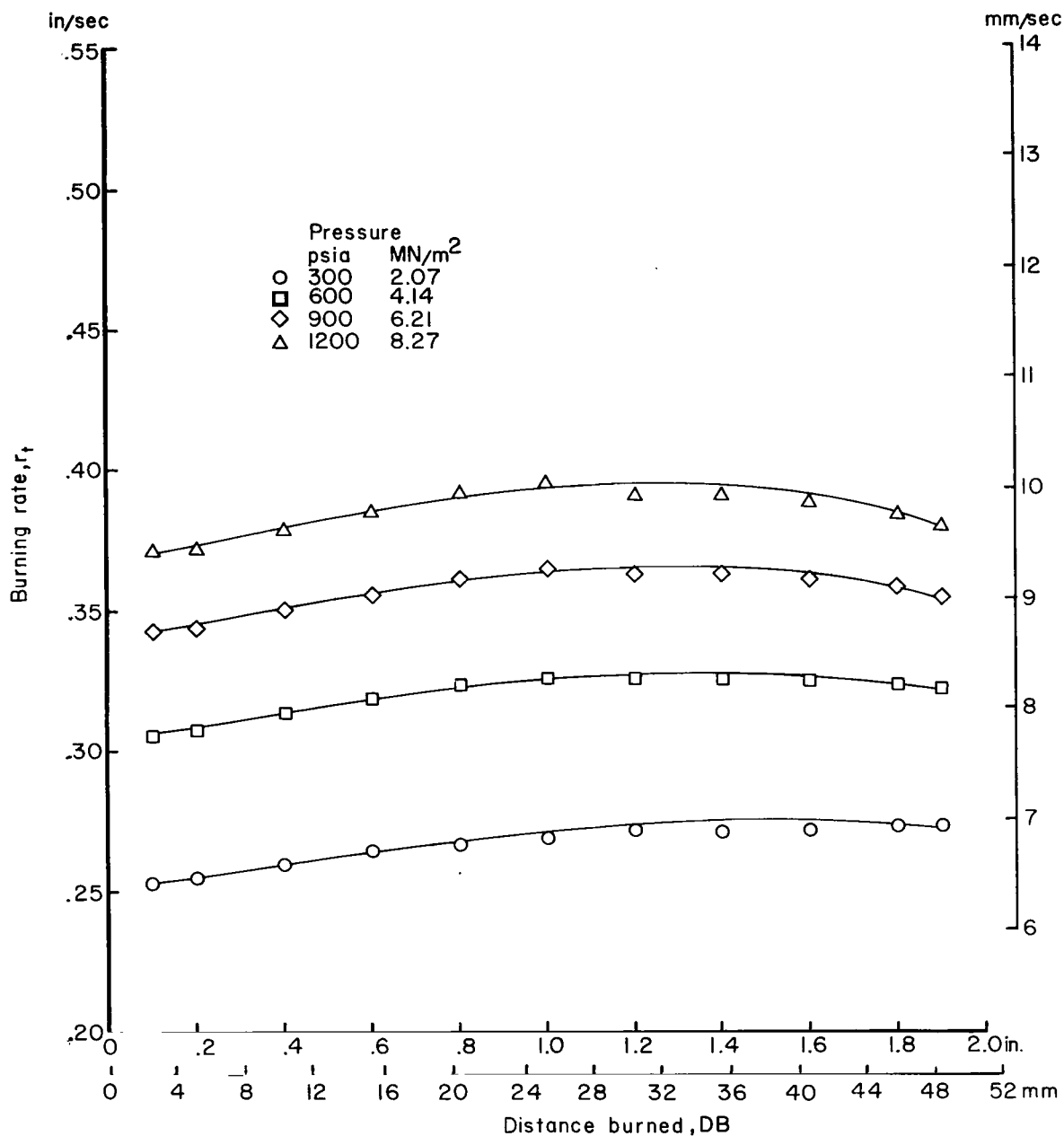
(a) 0g normal acceleration.

Figure 6.- Instantaneous burning-rate data.
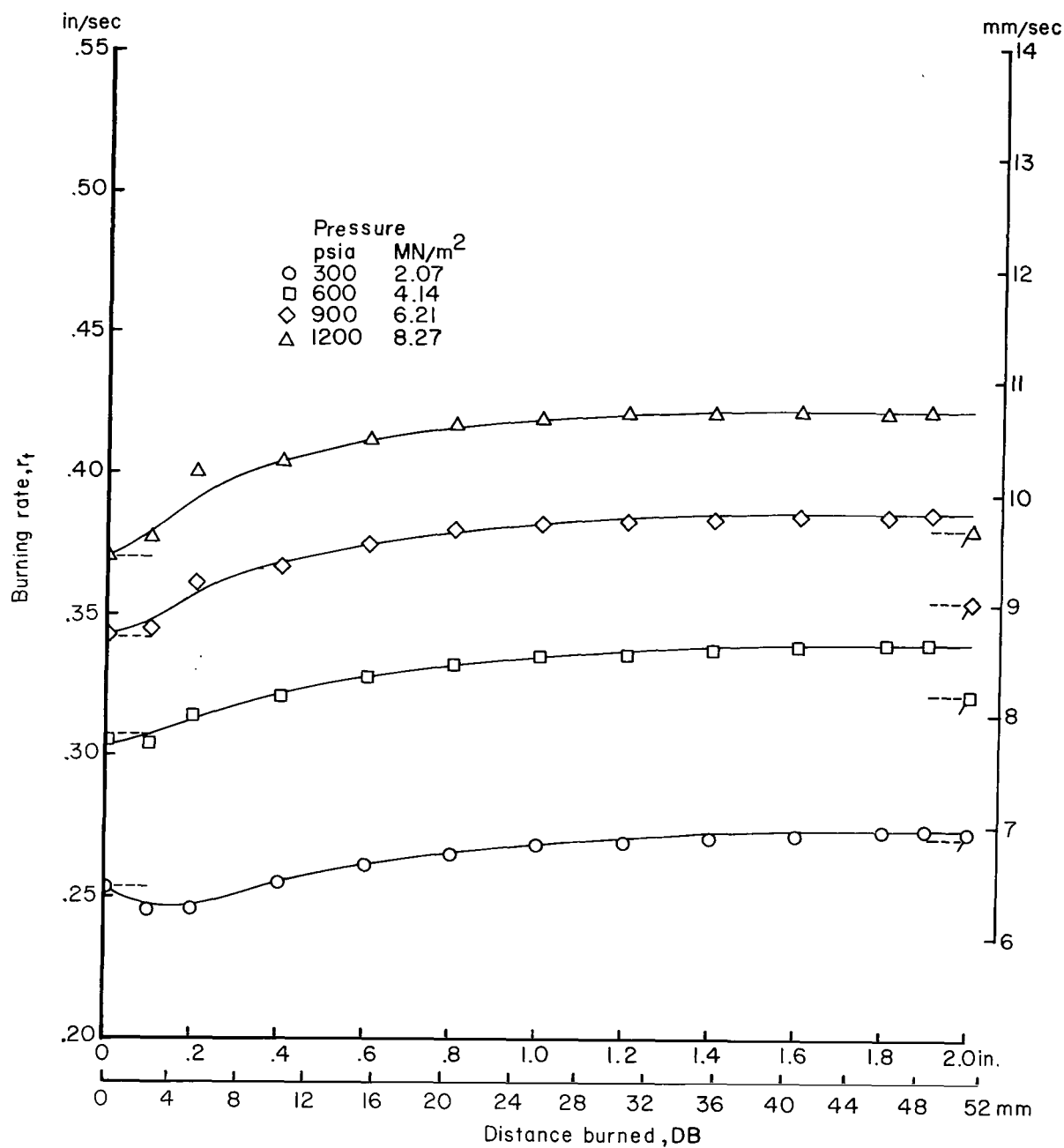
(b) 20g normal acceleration.
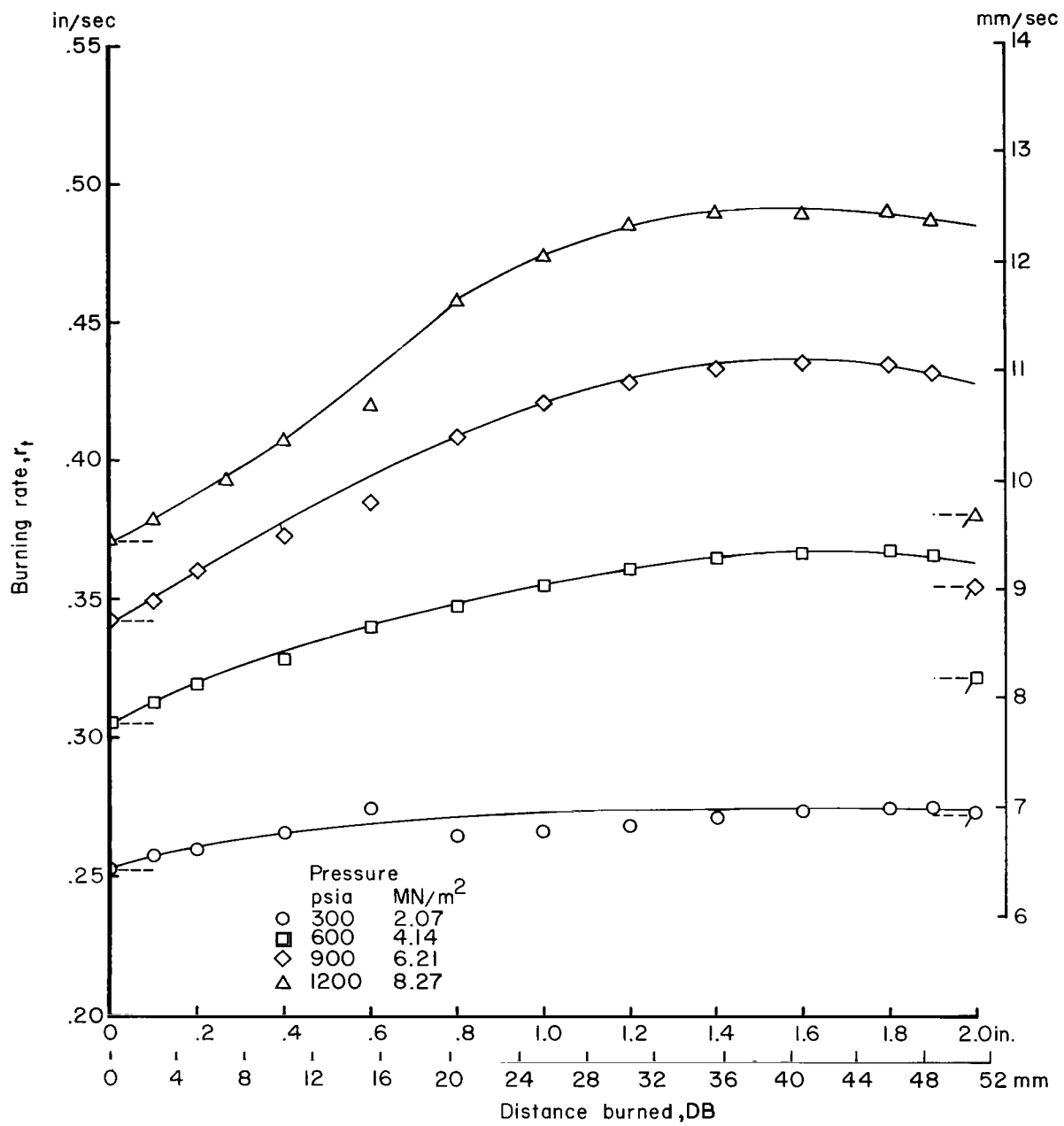
Figure 6.- Continued.

(c) 40g normal acceleration.
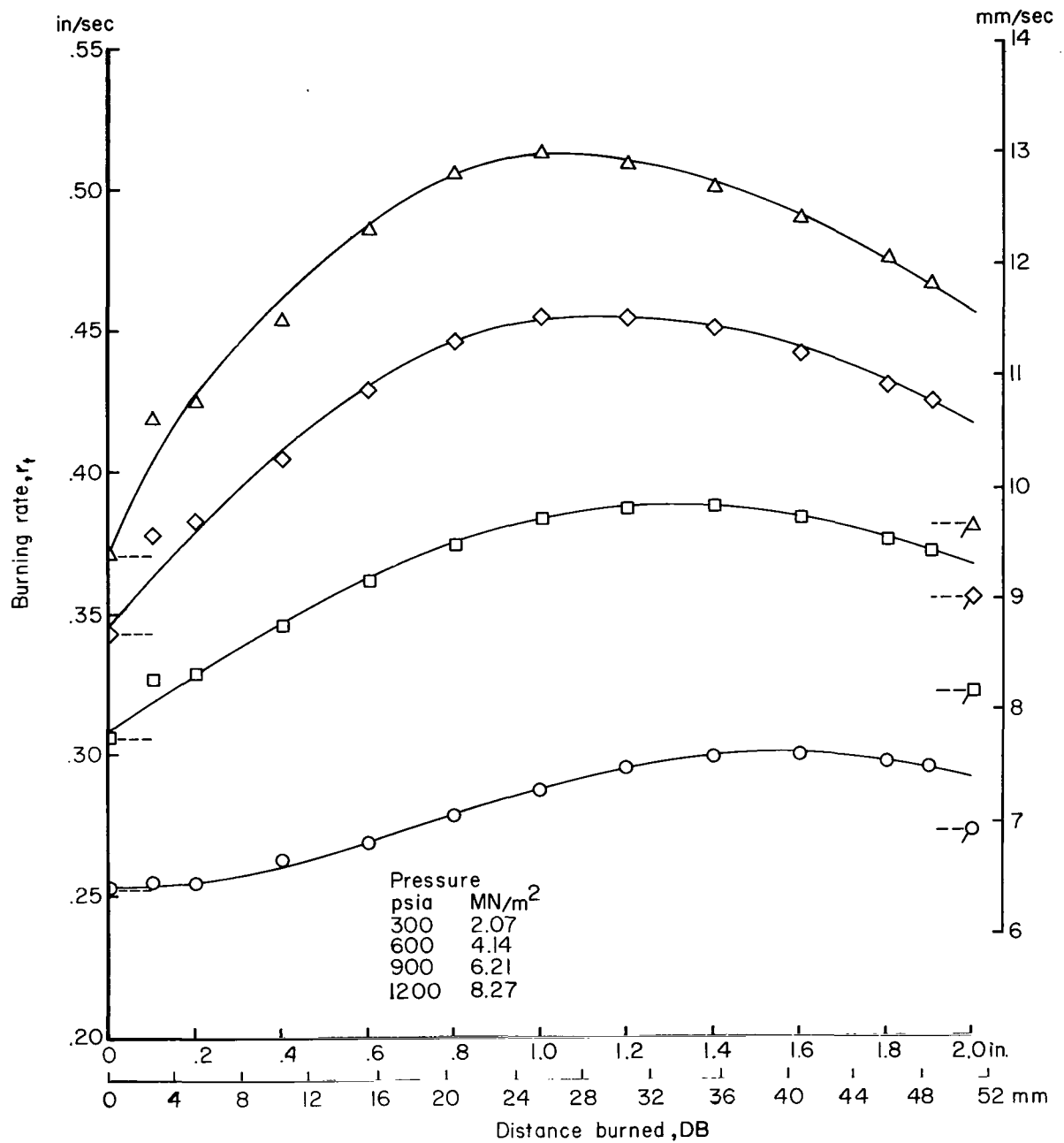
Figure 6.- Continued.

(d) 60g normal acceleration.
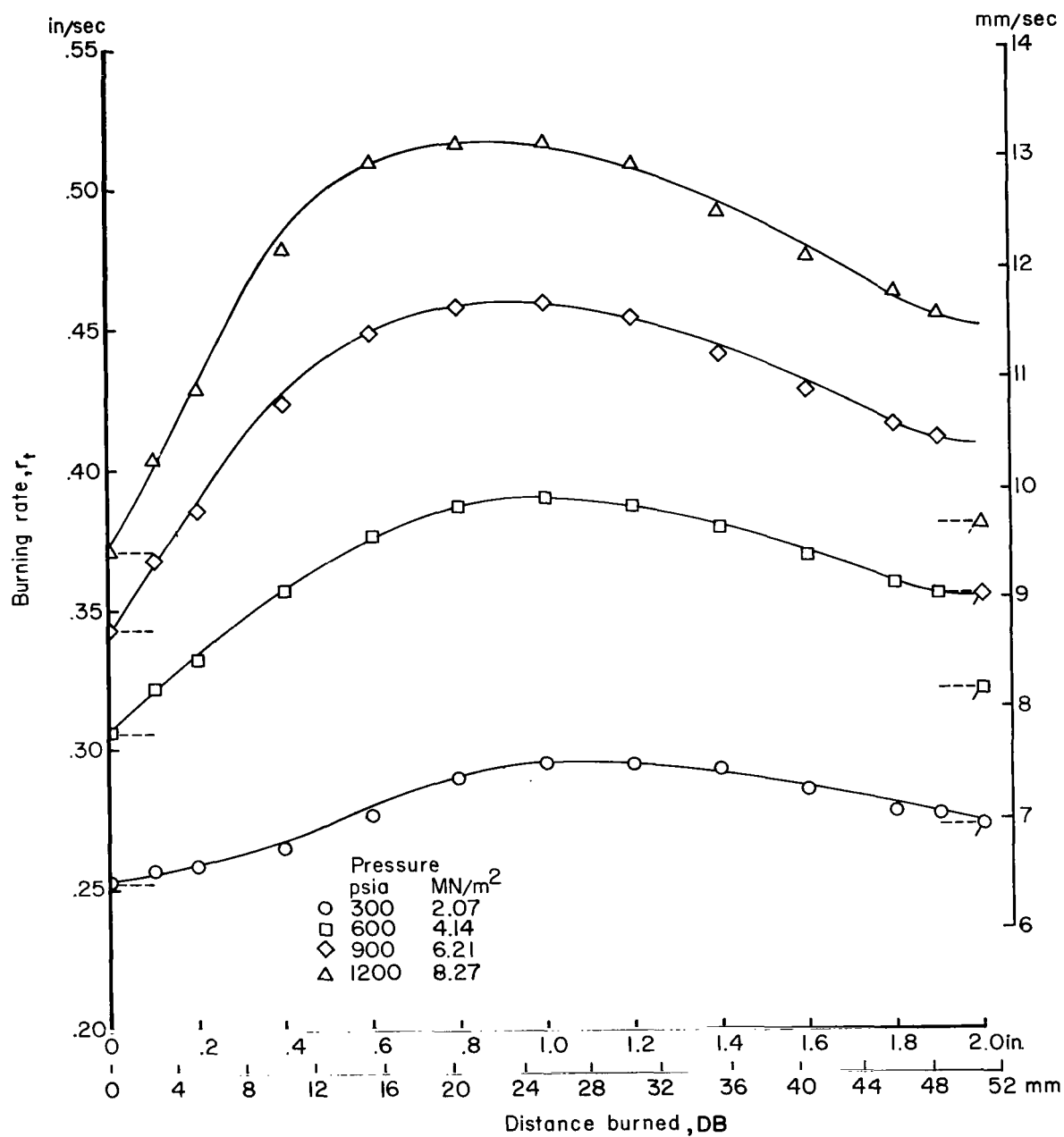
Figure 6.- Continued.

(e) 80g normal acceleration.
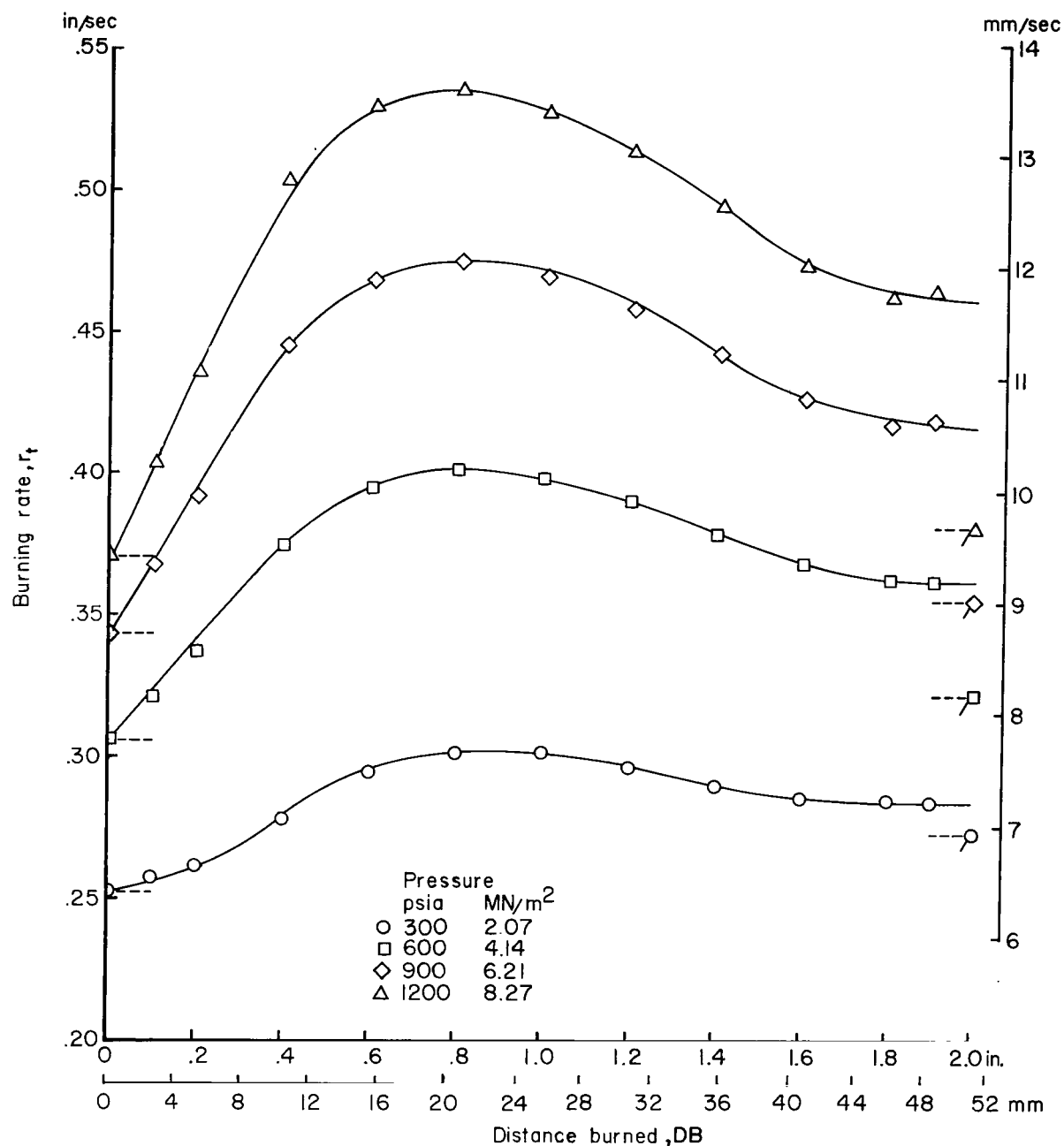
Figure 6.- Continued.

(f)   100g normal acceleration.
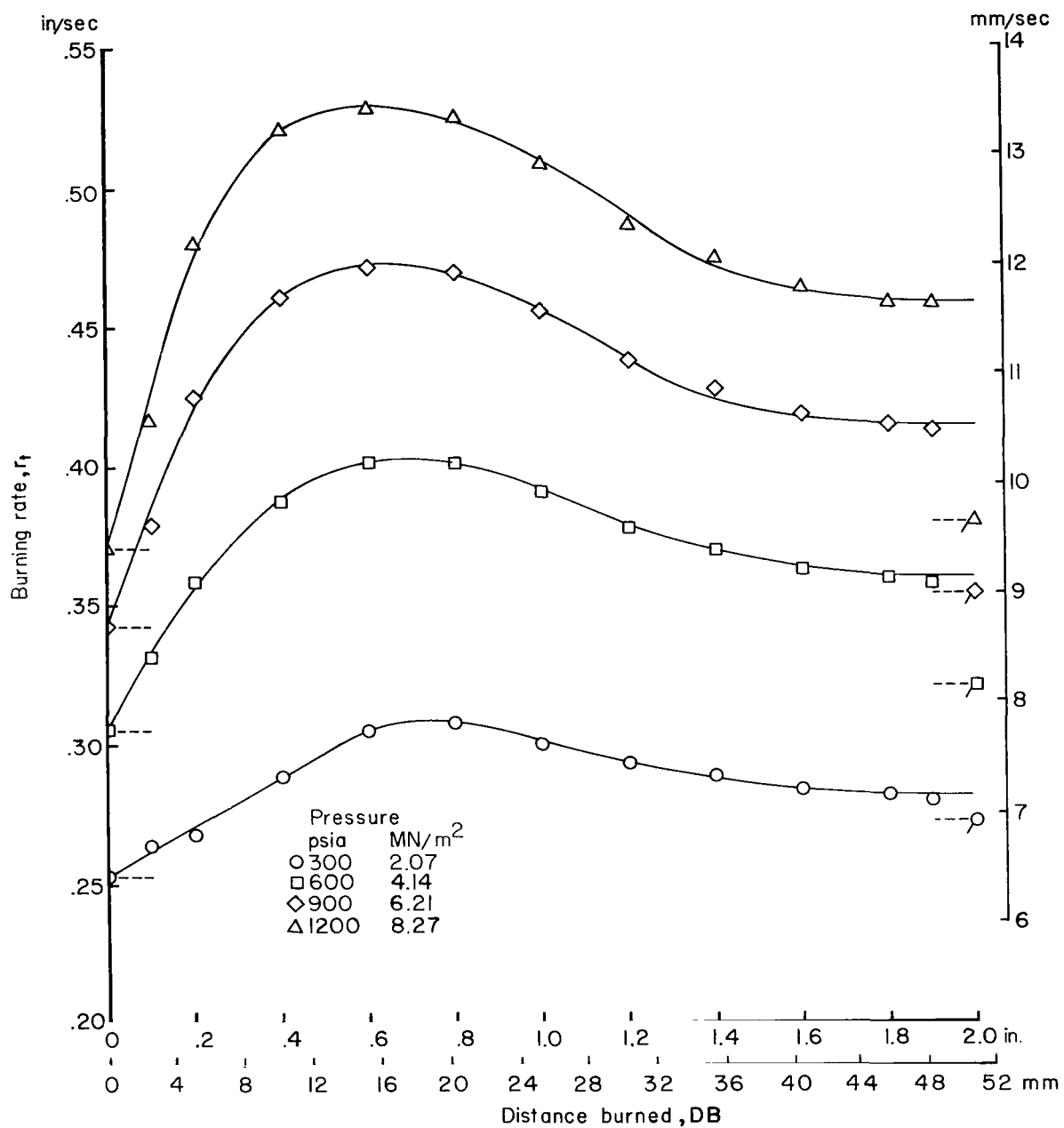
Figure 6.- Continued.

(g) 120g normal acceleration.

Figure 6.- Continued.
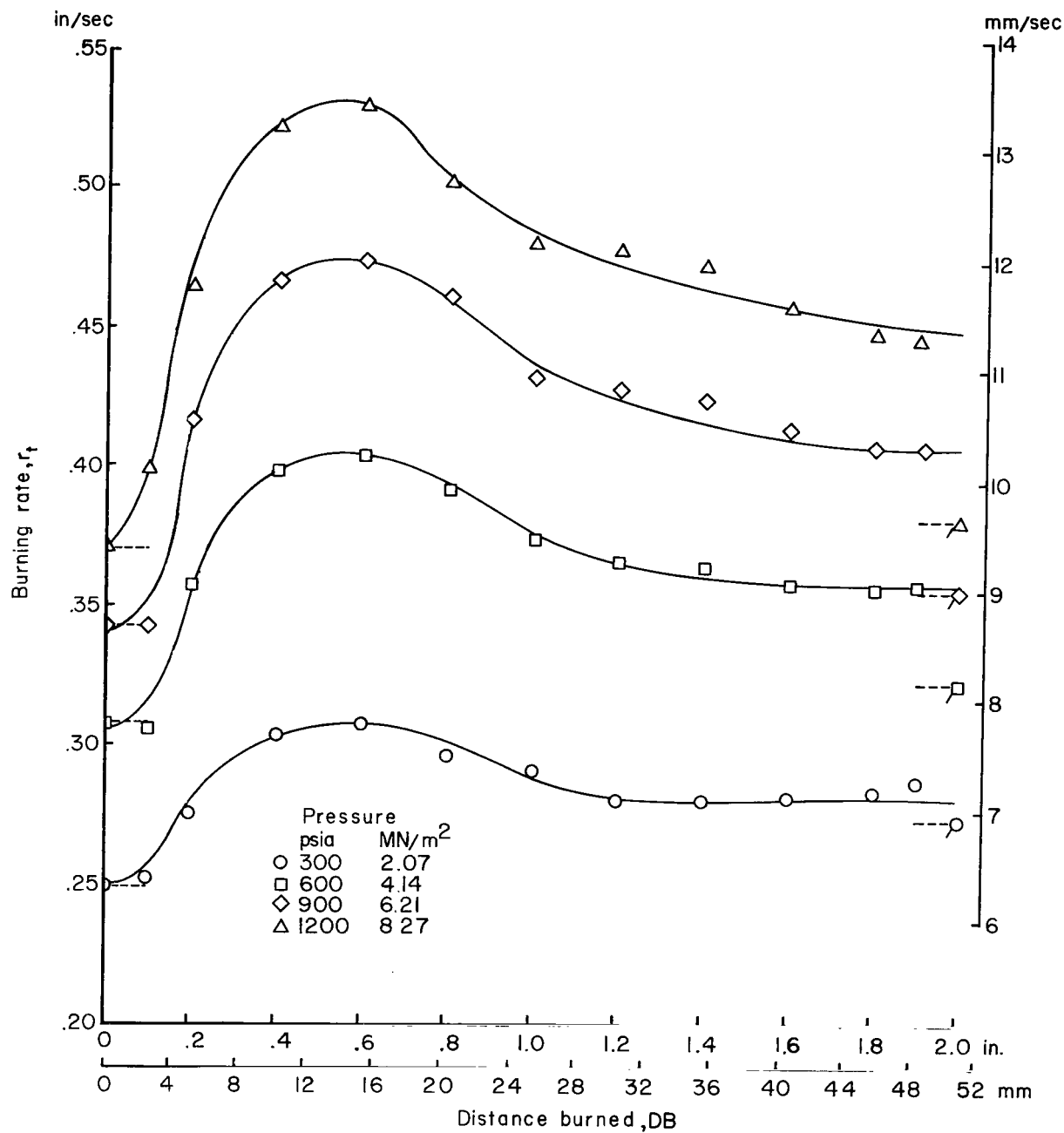
(h) 140g normal acceleration.

Figure 6.- Concluded.
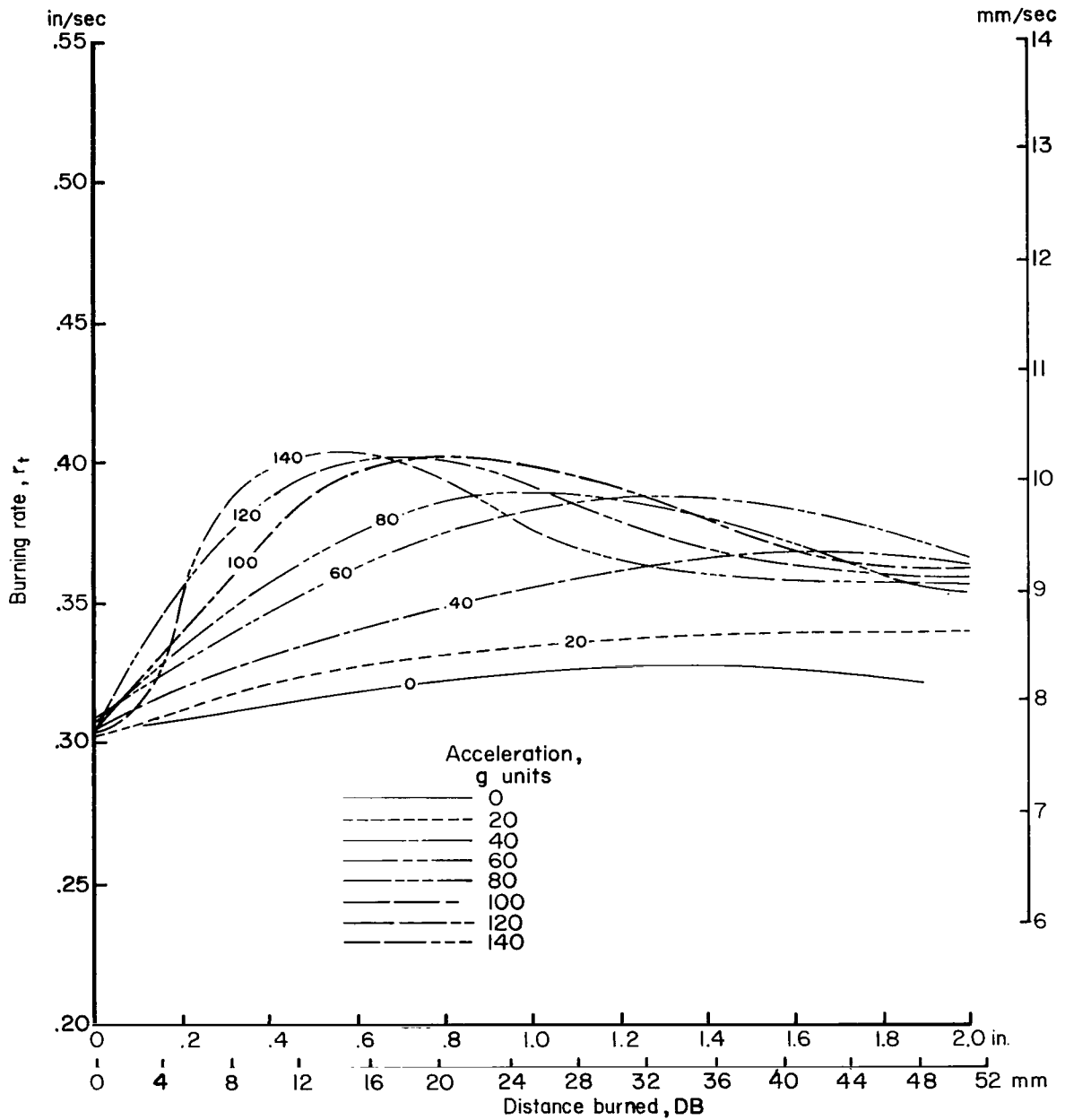
Figure 7.- Composite instantaneous burning-rate data at nominal chamber pressures of 4.14 MN/m^2 (600 psia).
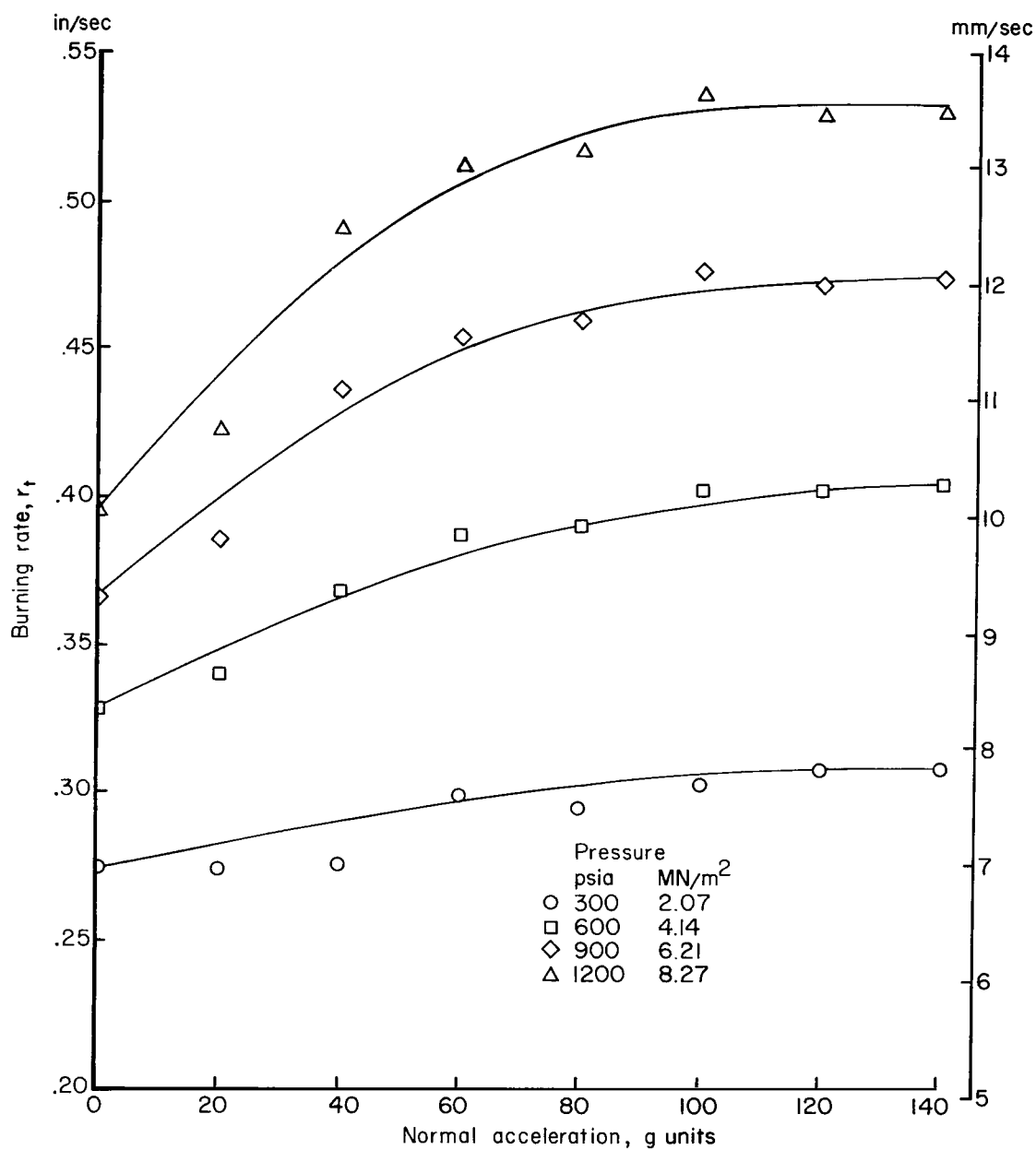
Figure 8.- Effect of acceleration on $r_{t,max}$.

Figure 9.- Distance burned to $r_{t,max}$ as a function of normal acceleration.
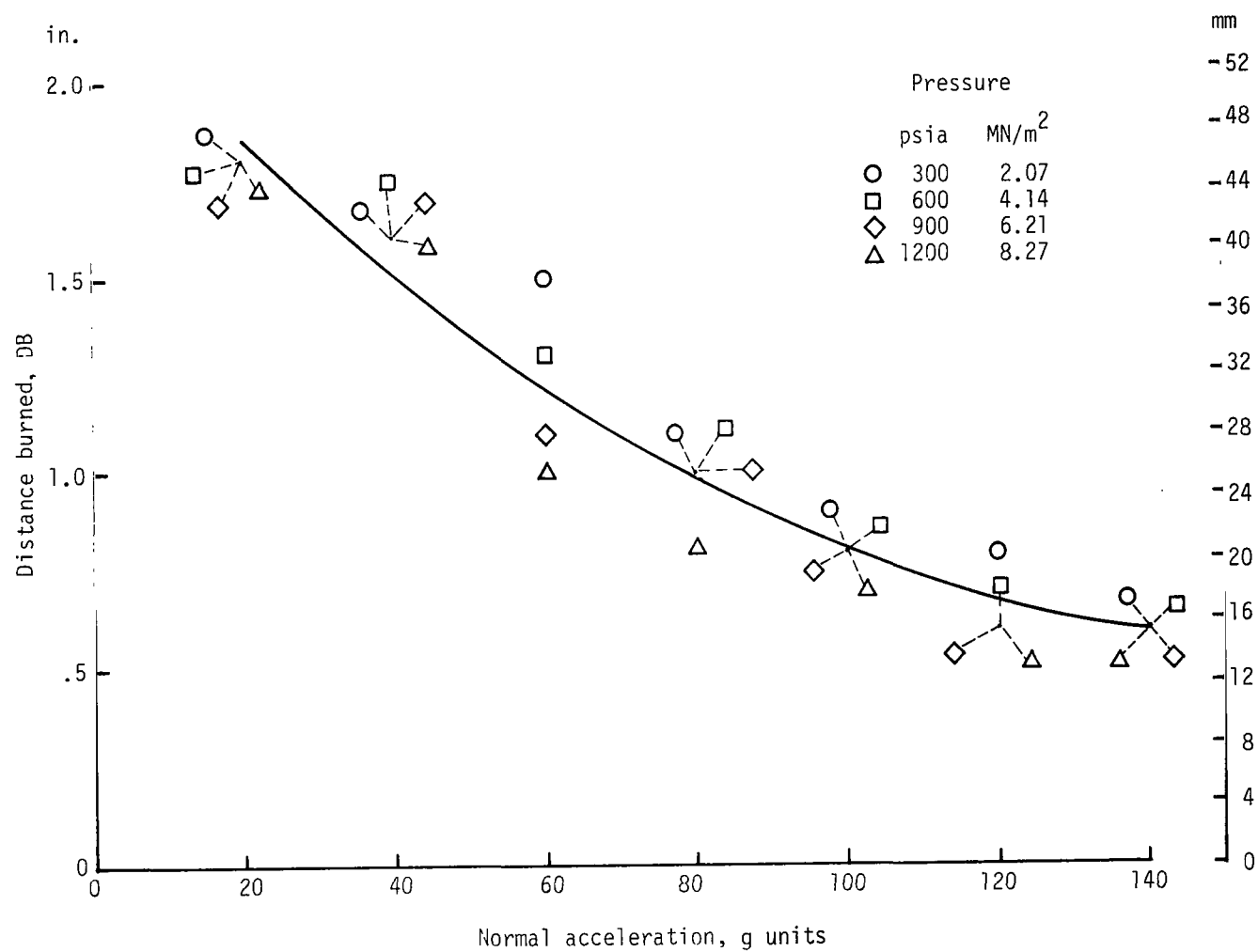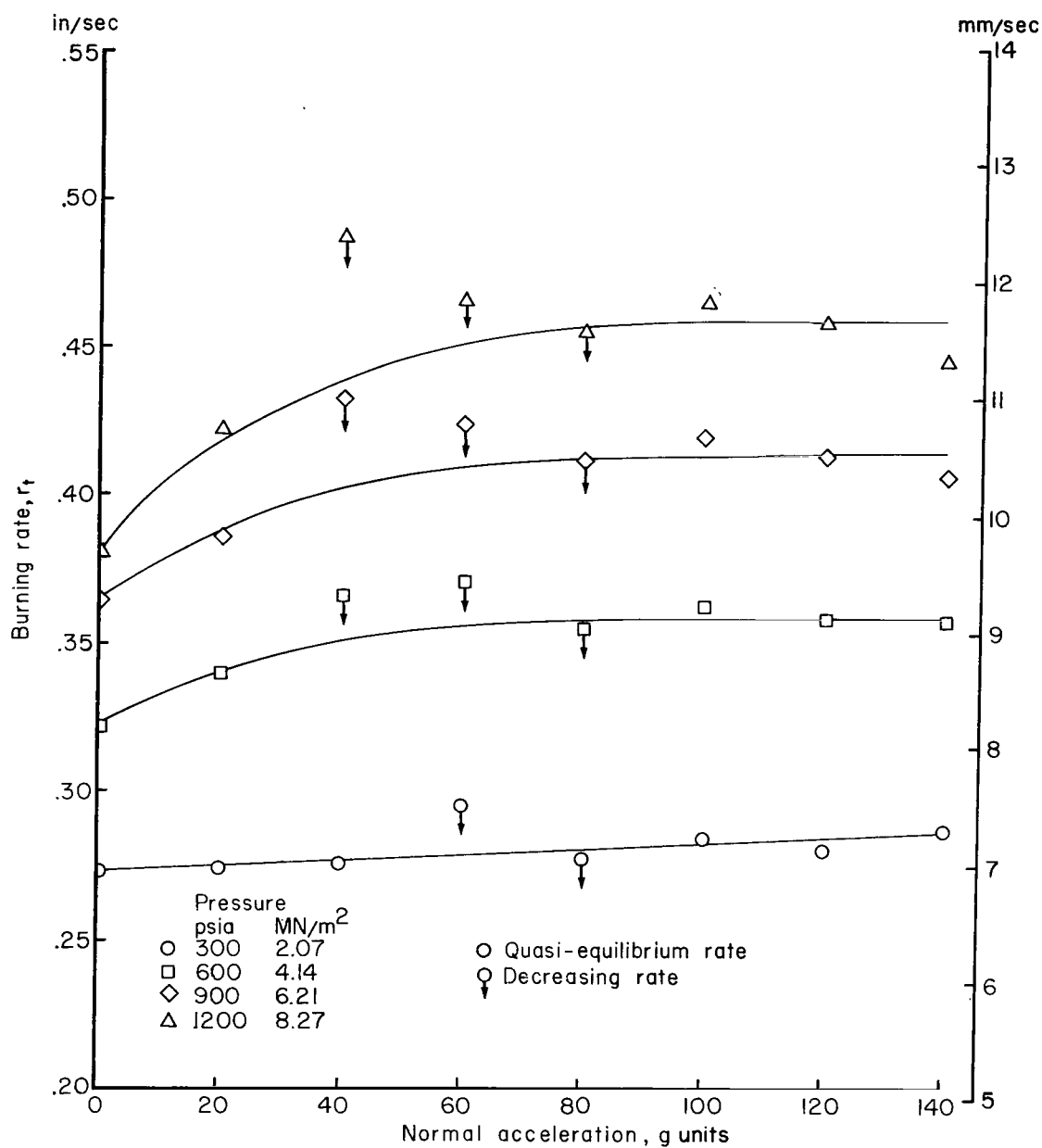
Figure 10.- Instantaneous burning rate at DB = 48.3 mm (1.9 in.) as a function of normal acceleration.
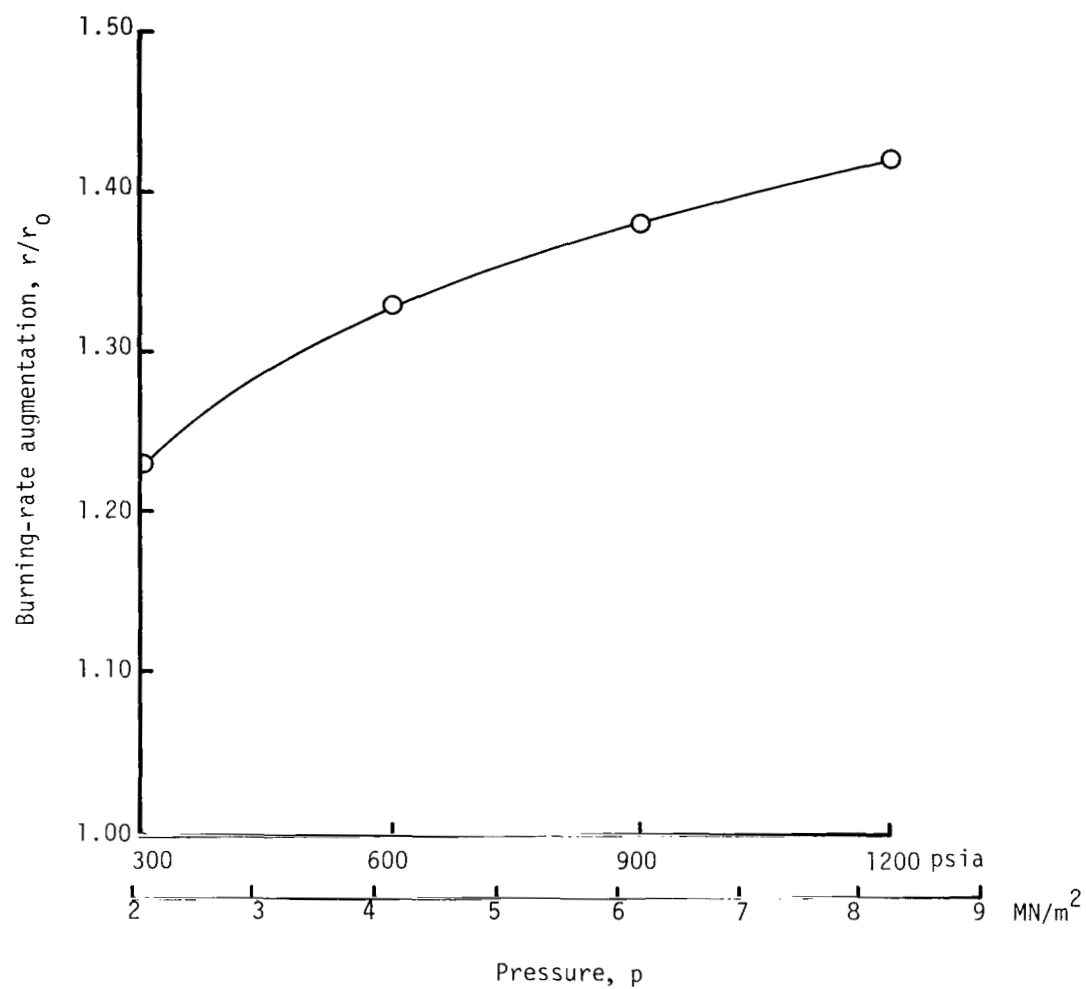
Figure 11.- Effect of pressure on maximum burning-rate augmentation at 140g.

	0%	100%	71%	72%	Spheres
	0%	0%	25%	0%	Buttons
	0%	0%	4%	28%	Irregular
	0%	0%	0%	0%	Sheets
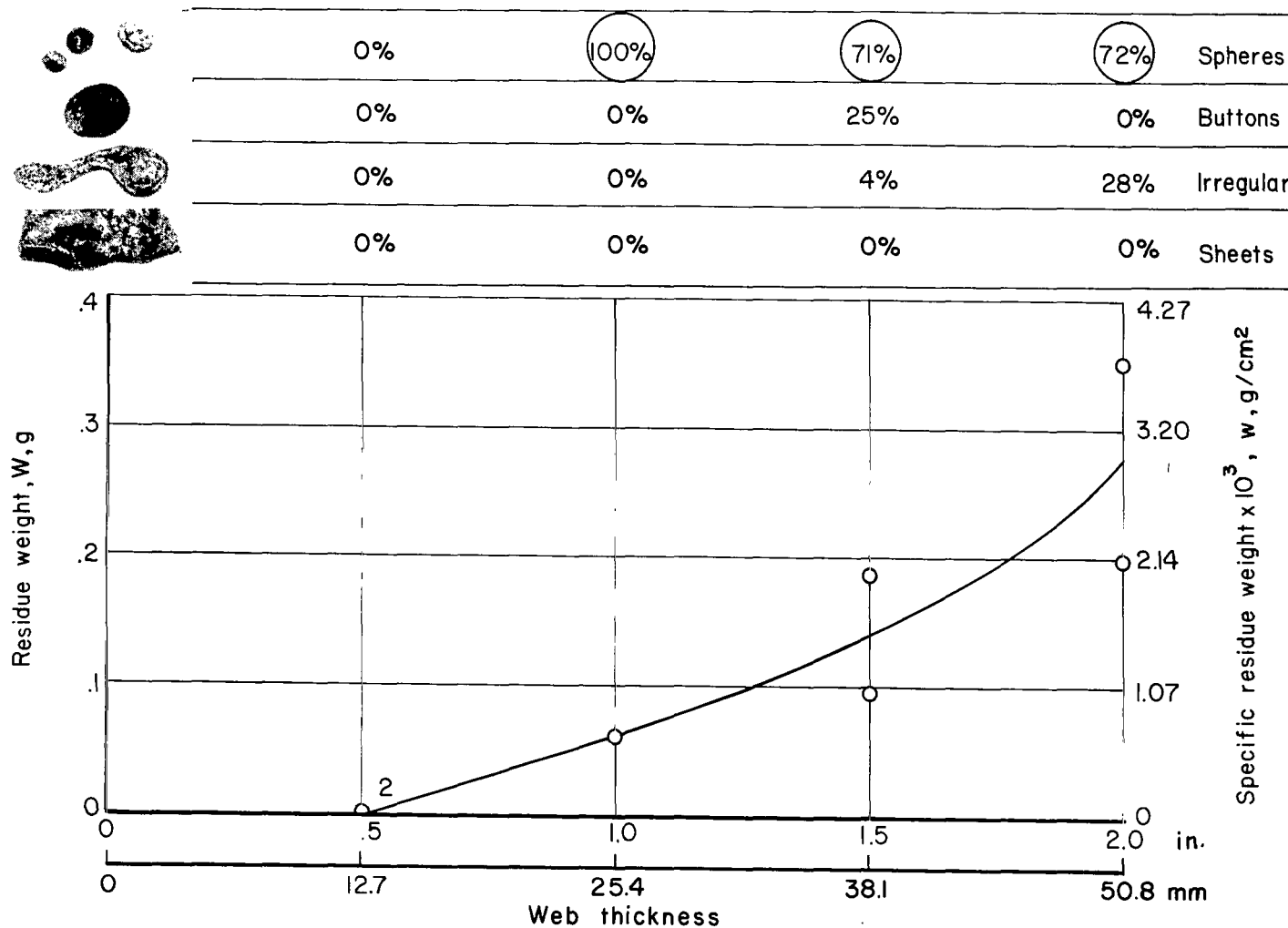
(a)   20g normal acceleration.

Figure 12.- Effect of propellant thickness on residue weight at nominal chamber pressures of 4.14 MN/m^2 (600 psia).
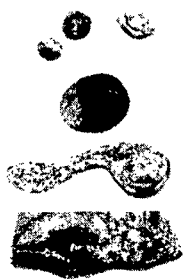
	58%	100%	97%	98%	Spheres
	0%	0%	0%	0%	Buttons
	42%	0%	3%	2%	Irregular
	0%	0%	0%	0%	Sheets
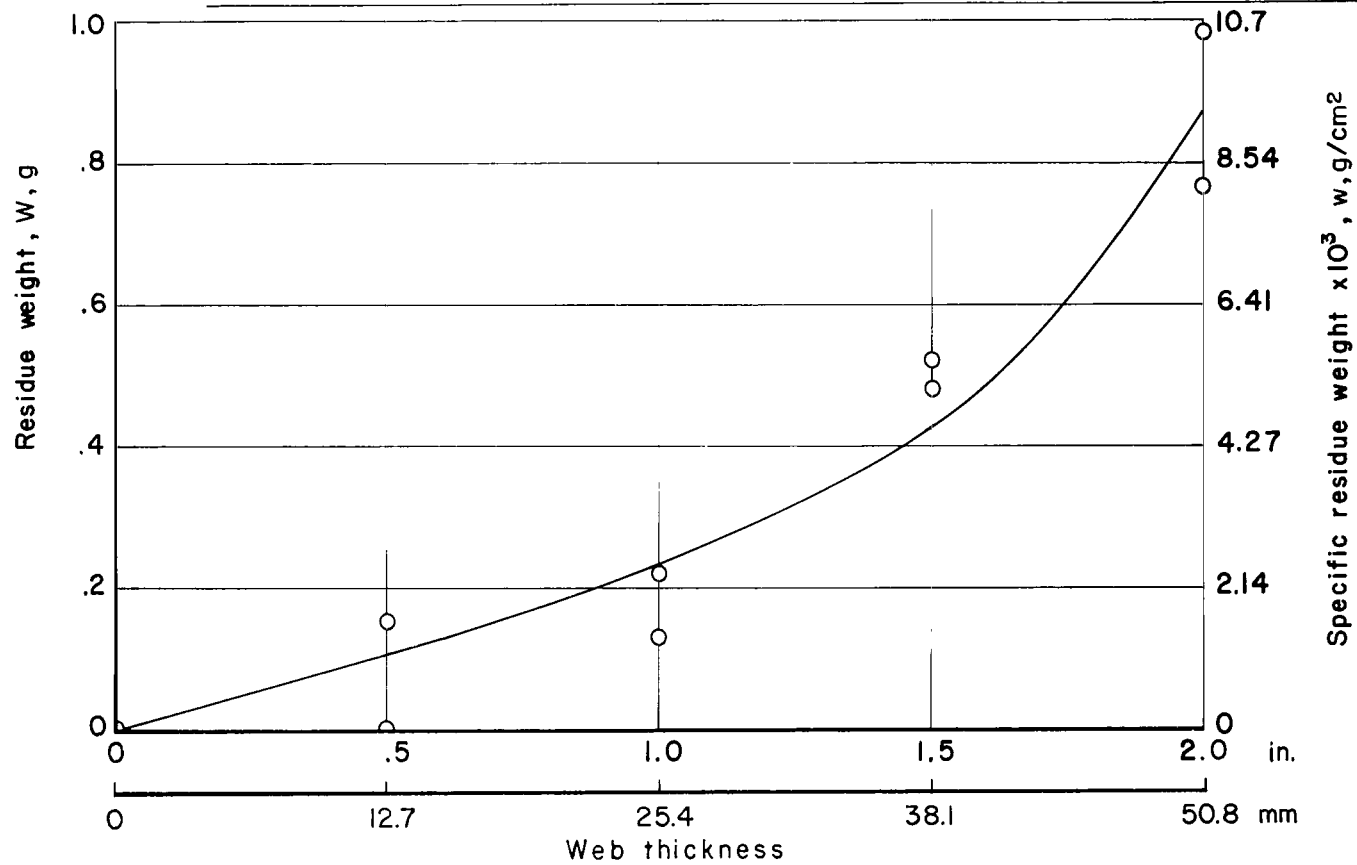
(b) 40g normal acceleration.

Figure 12.- Continued.

	100%	90%	75%	66%	Spheres
	0%	0%	25%	34%	Buttons
	0%	10%	0%	0%	Irregular
	0%	0%	0%	0%	Sheets
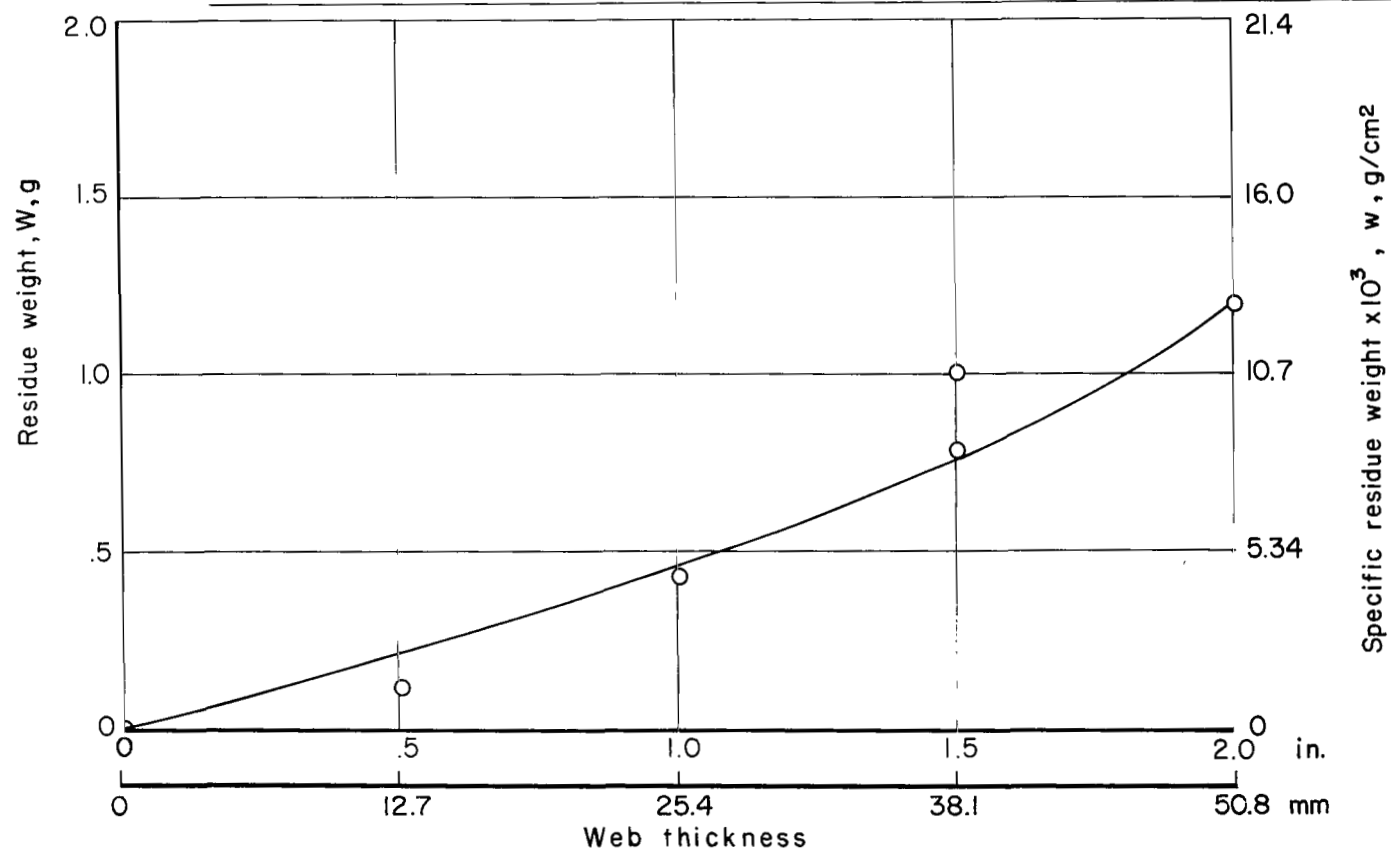
(c) 60g normal acceleration.

Figure 12.- Continued.

89%	86%	25%	20%	Spheres
0%	14%	75%	48%	Buttons
11%	0%	0%	32%	Irregular
0%	0%	0%	0%	Sheets
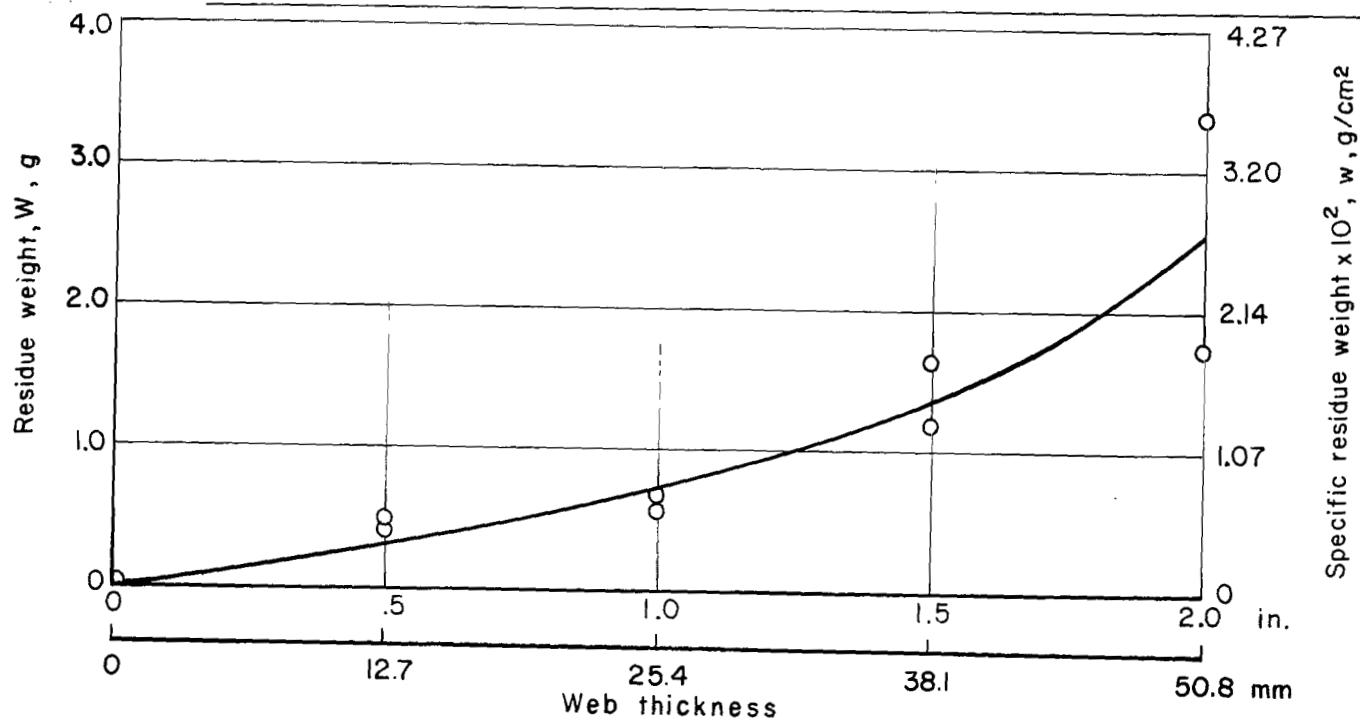
(d) 80g normal acceleration.

Figure 12.- Continued.

(84%)	(92%)	(60%)	0%	Spheres
0%	6%	31%	27%	Buttons
0%	2%	9%	(41%)	Irregular
16%	0%	0%	32%	Sheets
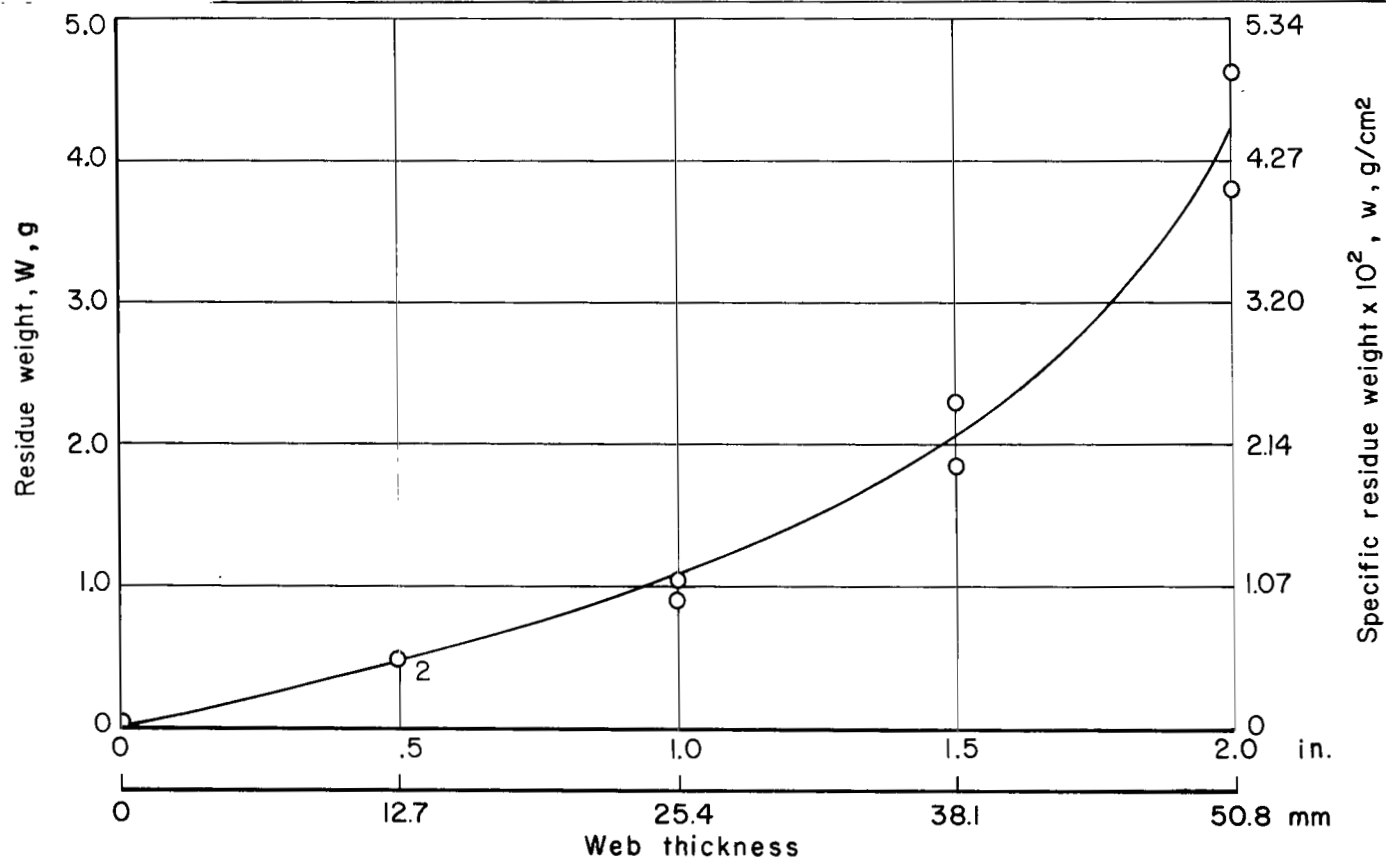
(e)   100g normal acceleration.

Figure 12.- Continued.

(100%)	(82%)	0%	0%	Spheres
0%	18%	(43%)	14%	Buttons
0%	0%	18%	0%	Irregular
0%	0%	39%	(86%)	Sheets
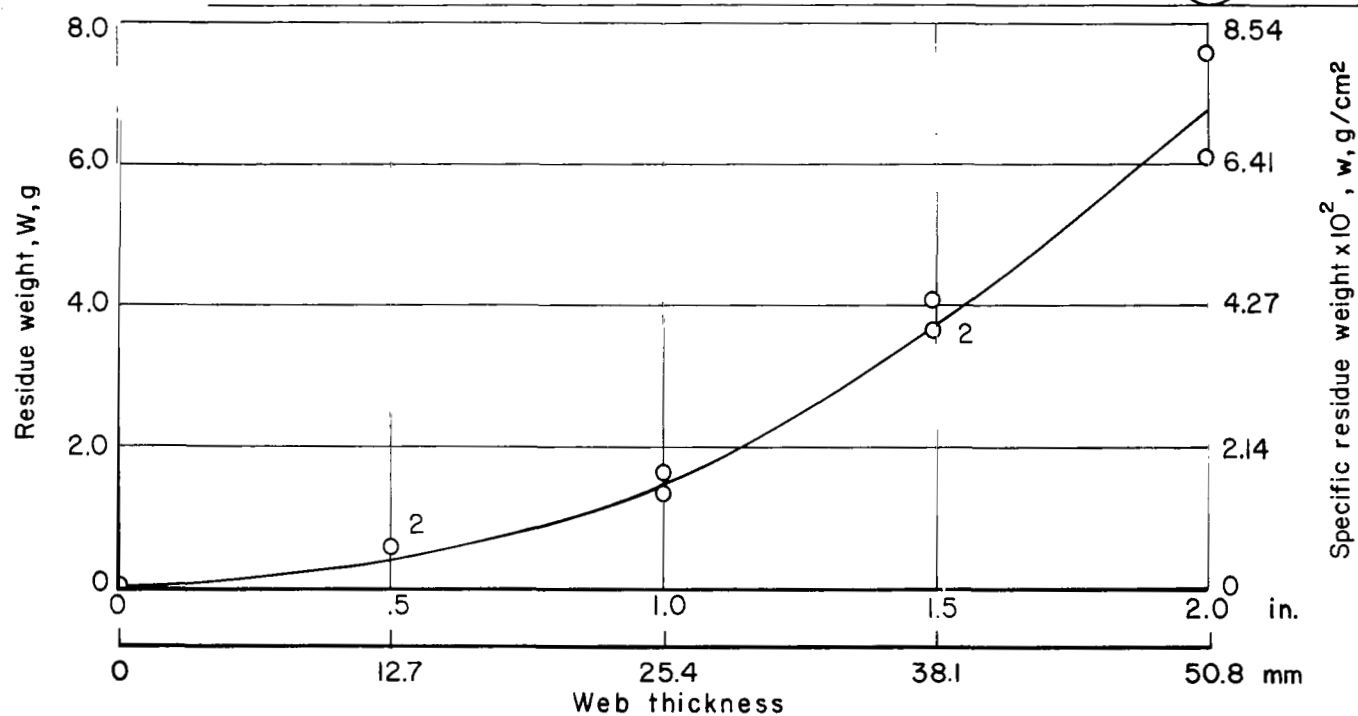
(f)   120g normal acceleration.

Figure 12.- Continued.

	95%	0%	0%	0%	Spheres
	0%	95%	20%	5%	Buttons
	0%	5%	0%	0%	Irregular
	5%	0%	80%	95%	Sheets
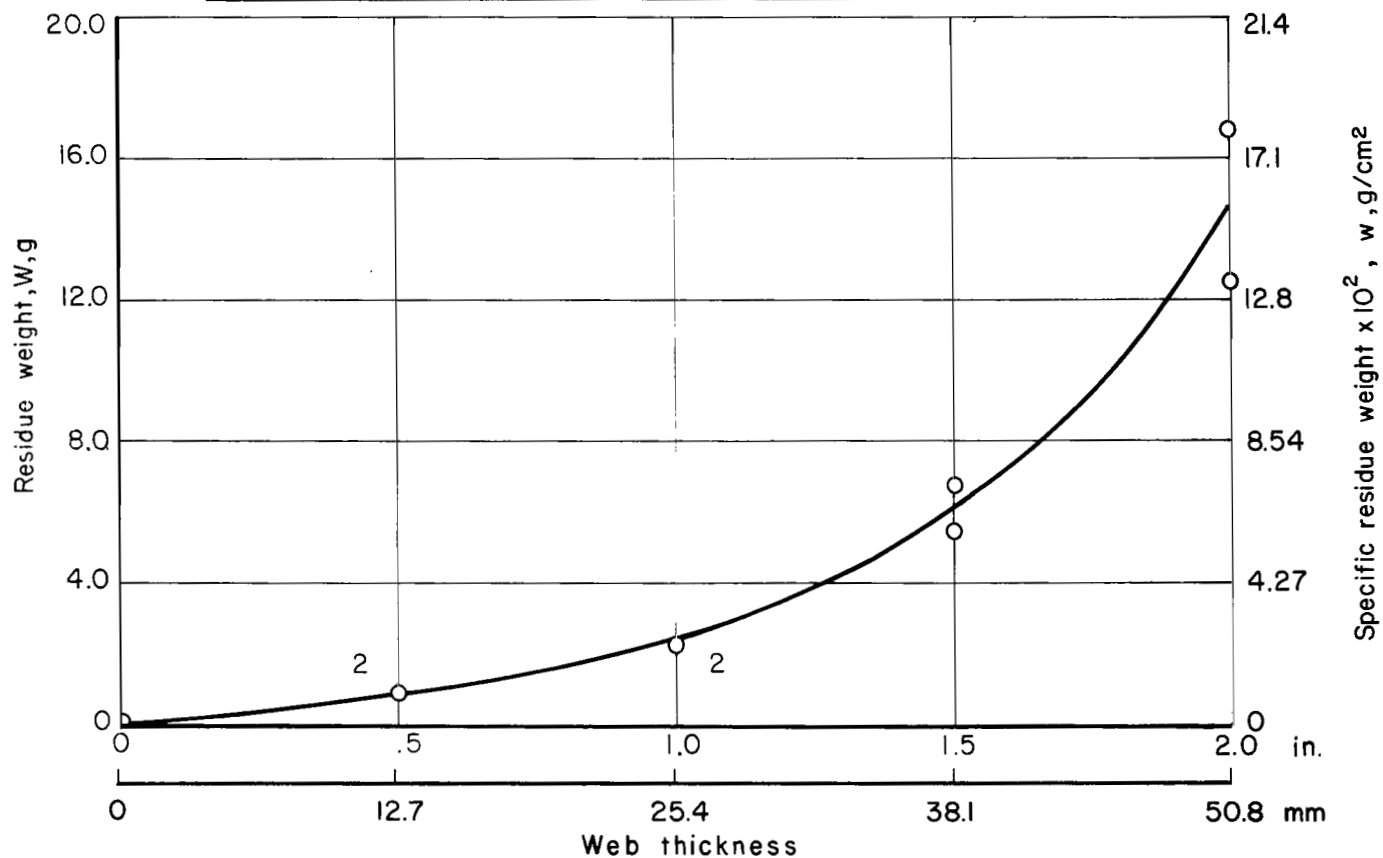
(g)   140g normal acceleration.

Figure 12.- Concluded.

72%	98%	66%	20%	0%	0%	0%	Spheres
0%	2%	34%	48%	27%	14%	5%	Buttons
28%	0%	0%	32%	41%	0%	0%	Irregular
0%	0%	0%	0%	32%	86%	95%	Sheets
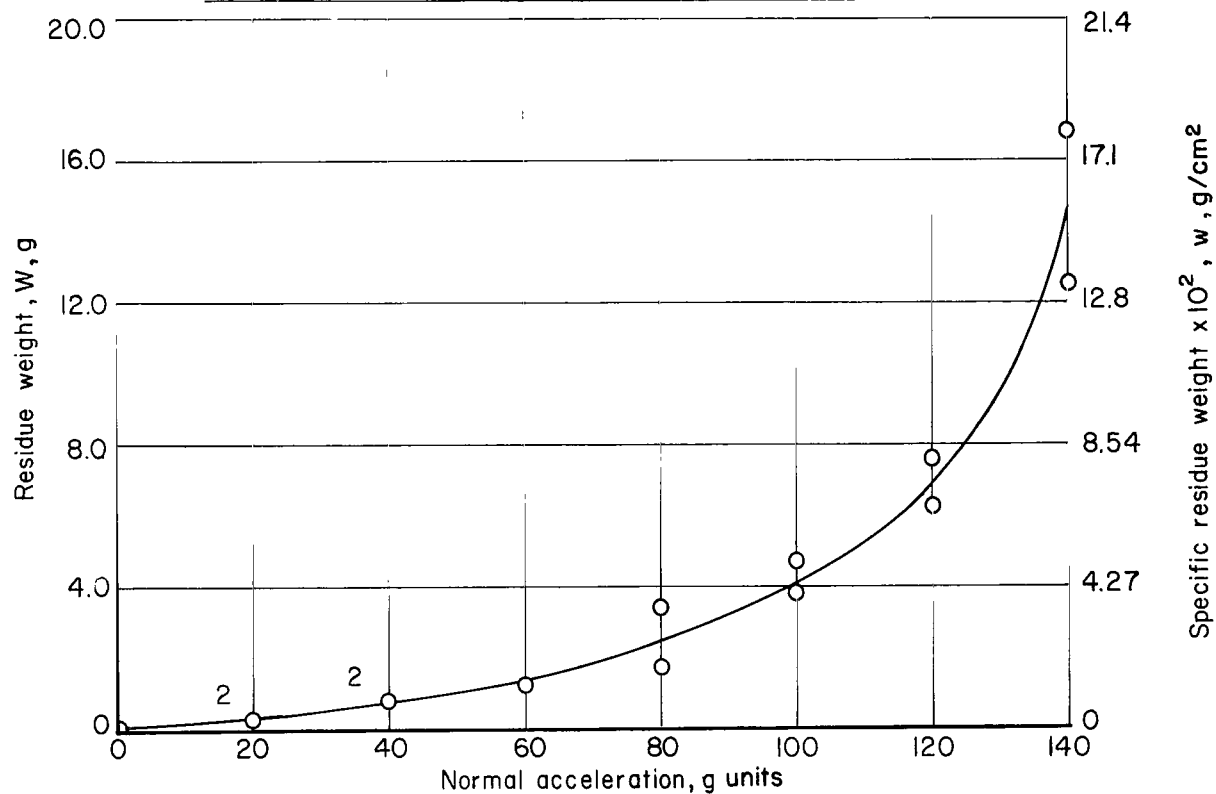
Figure 13.- Effect of normal acceleration on 5.08-cm (2.0 in.) web motor residue weight at nominal chamber pressures of 4.14 MN/m^2 (600 psia).
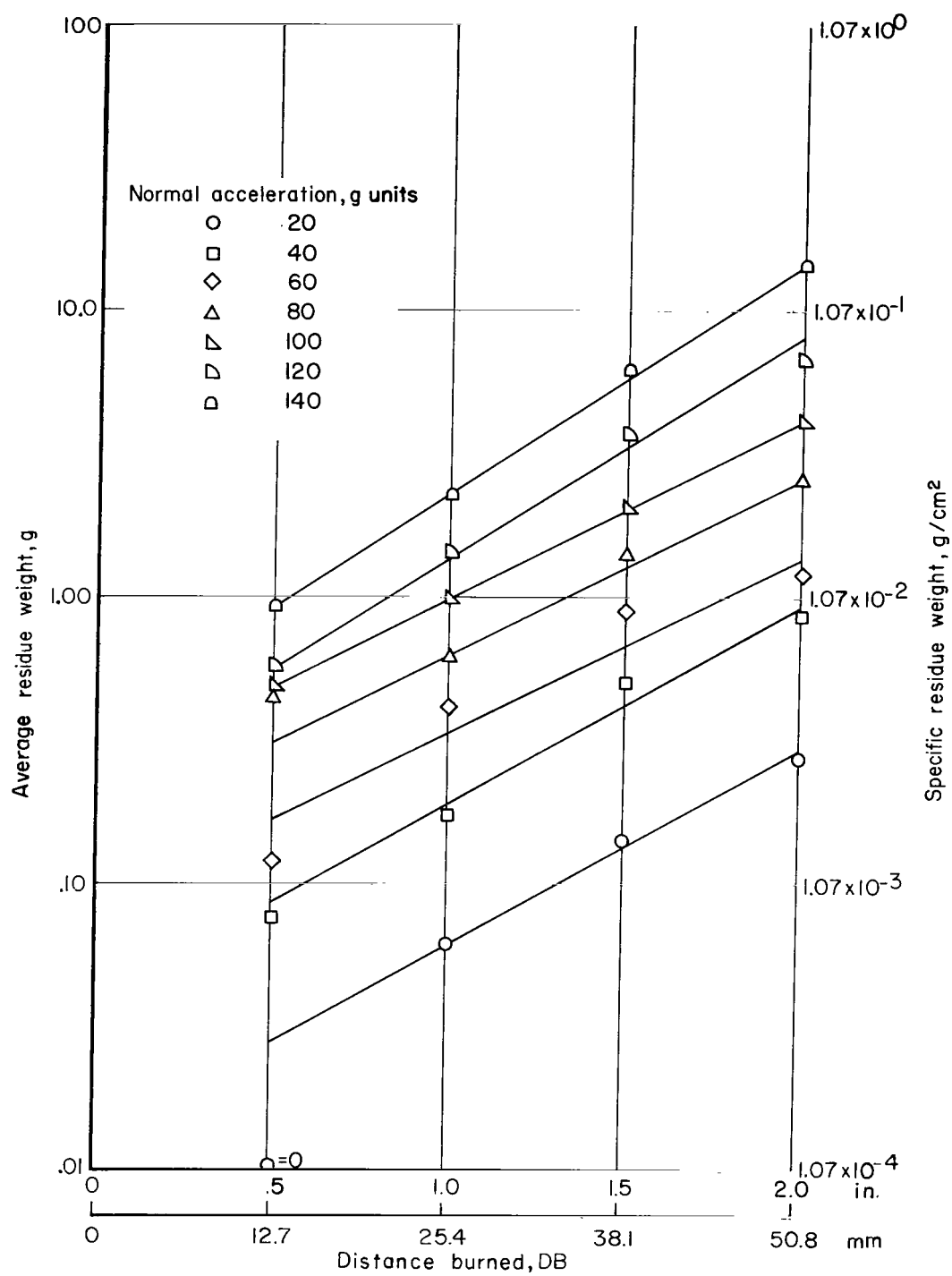
Figure 14.- Average residue weight as a function of distance burned with acceleration as a parameter.
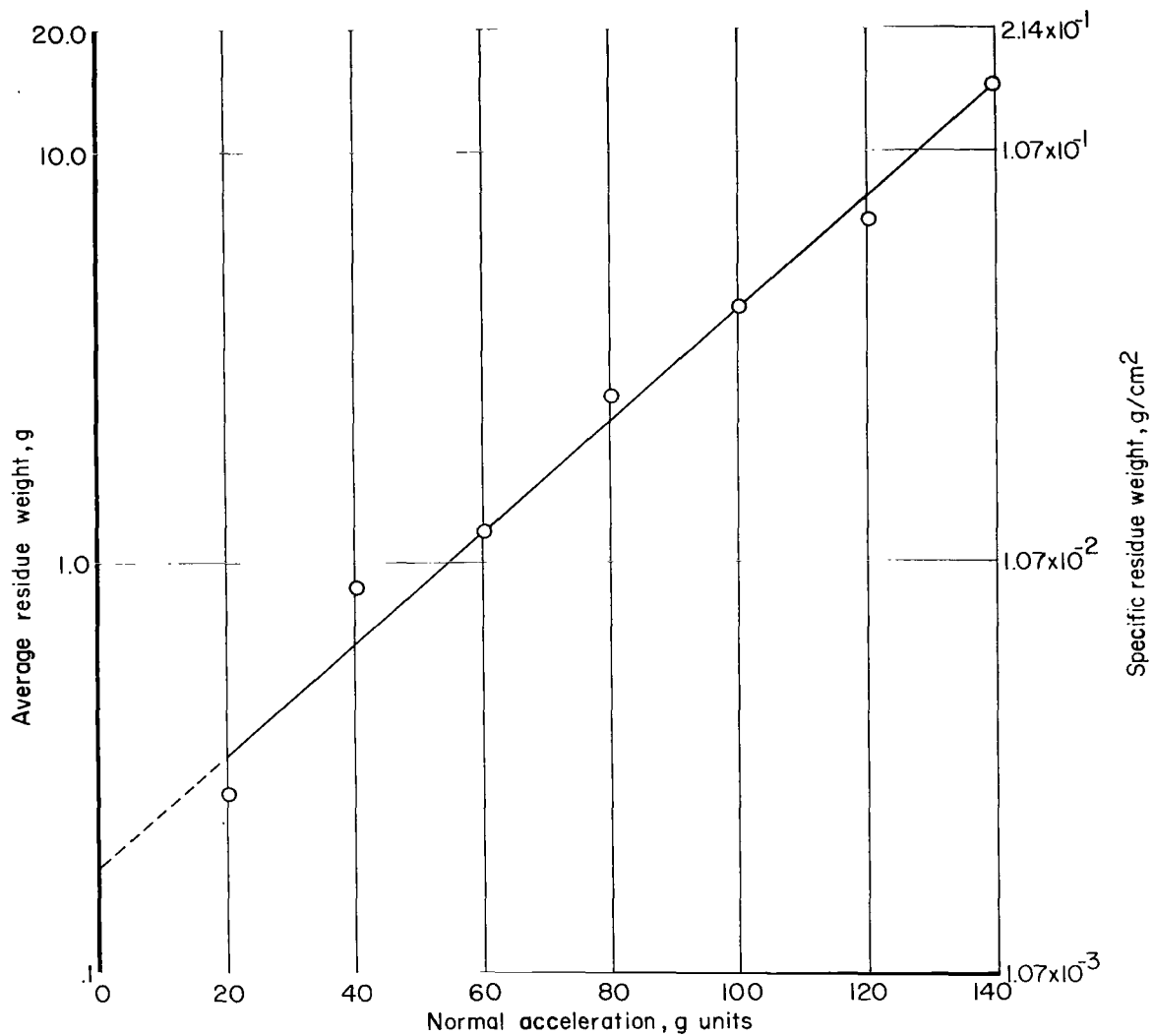
Figure 15.- Average residue weight as a function of normal acceleration for 5.08-cm (2.0 in.) web motor at nominal chamber pressures of 4.14 MN/m^2 (600 psia).
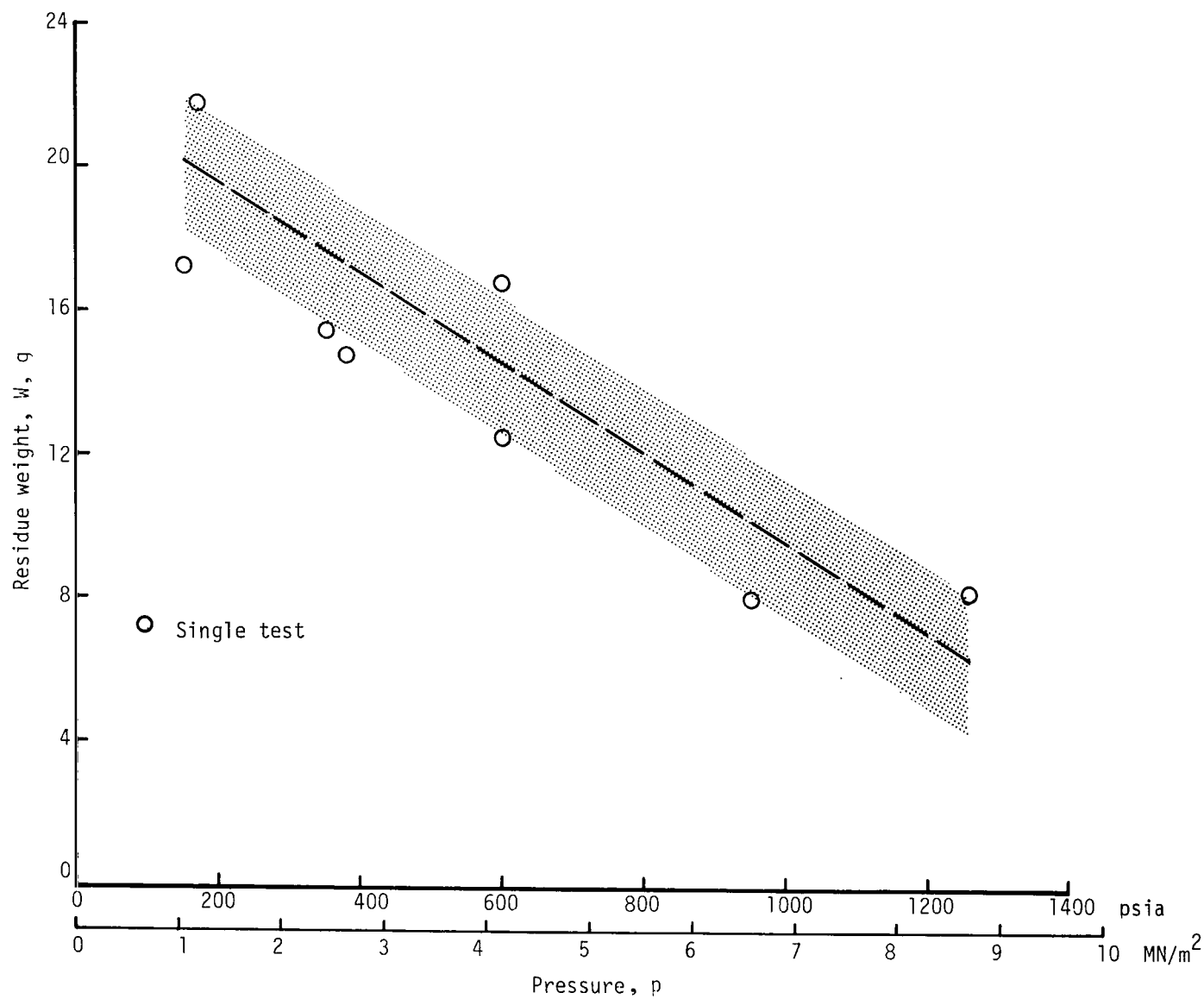
Figure 16.- Effect of pressure on residue weight at 140g normal acceleration.
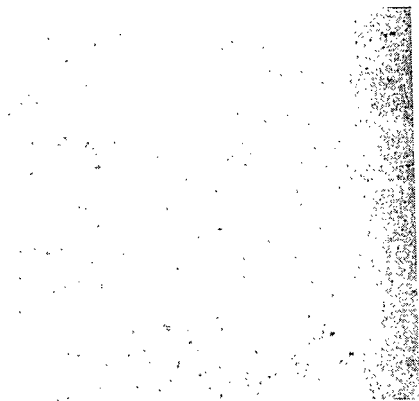
Static, DB=1.0in.(25.4mm), t=3.0sec
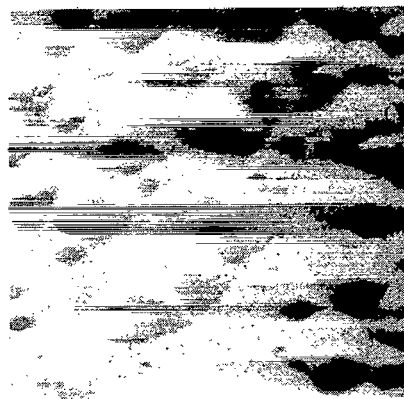
40g, DB=1.5in.(38.1mm), t=5.0sec
Bimodal
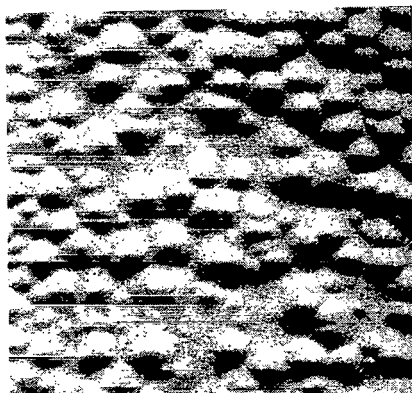
60g, DB=1.0in.(25.4mm), t=2.75sec
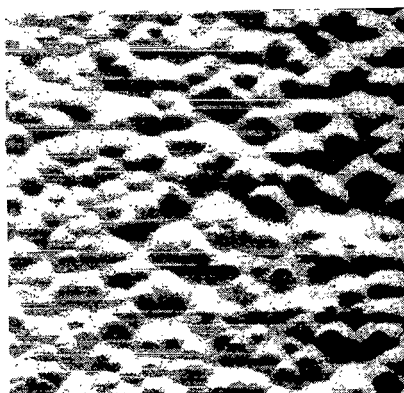
80g, DB=0.9 in.(22.9mm), t=2.5sec
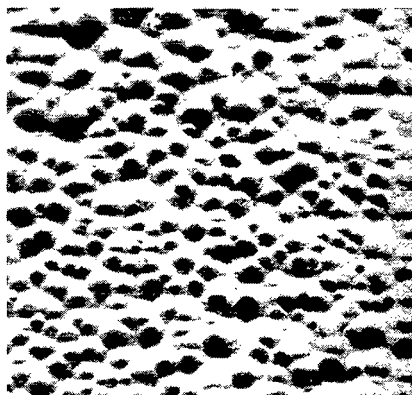
100g, DB=0.8in.(20.3mm), t=2.0sec
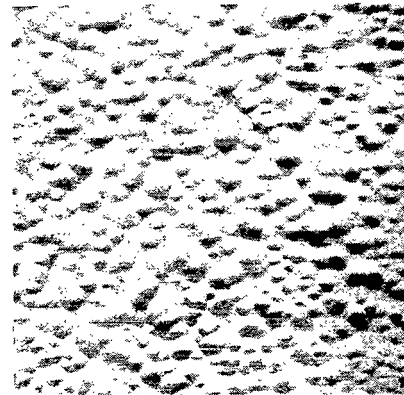
120g, DB=0.6in.(15.2mm), t=1.5sec

25.4mm
(1.0in.)
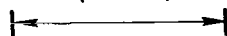
Figure 17.- Photographs of extinguished propellant surface at time of maximum
burning rate for various normal accelerations.
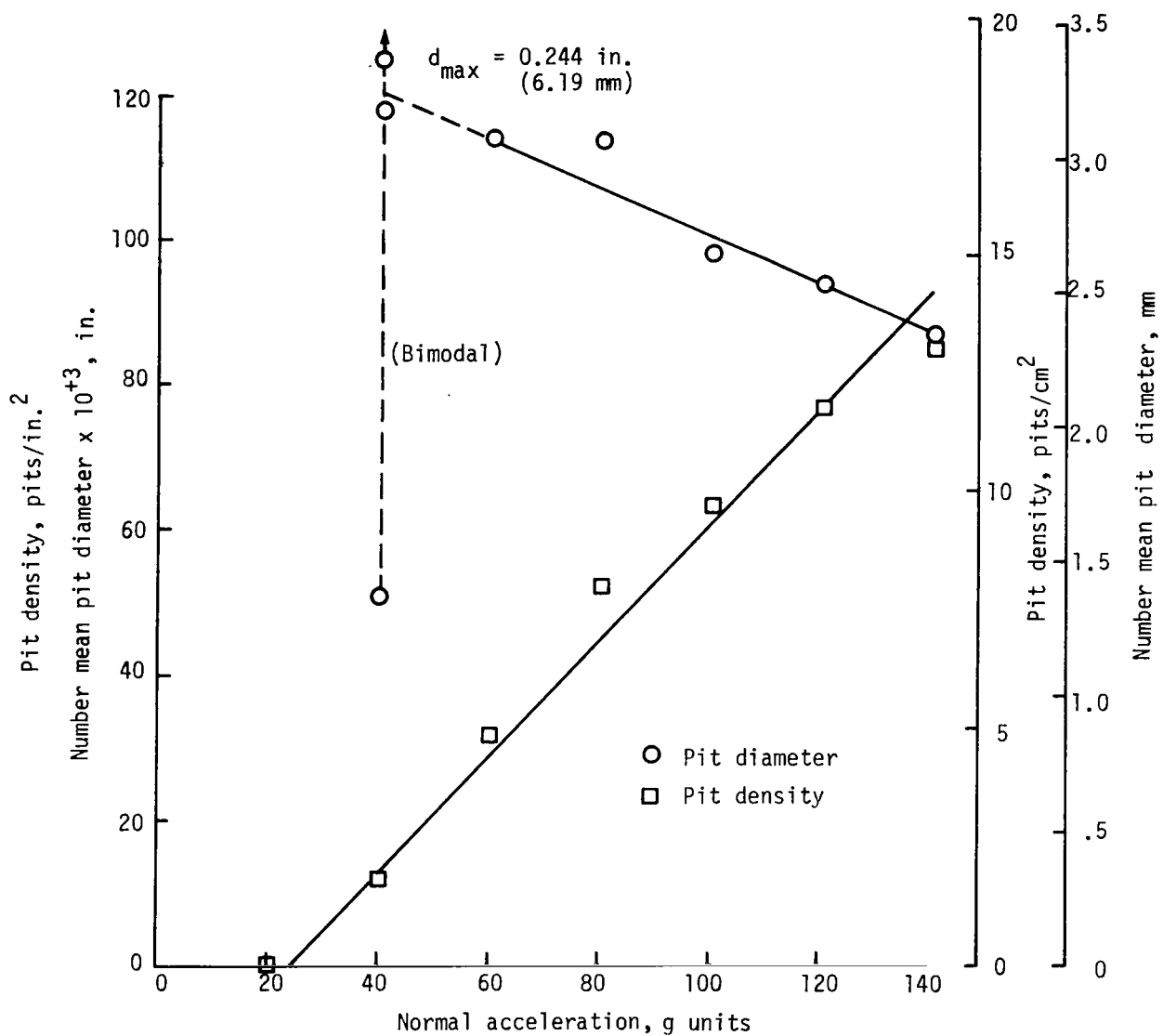
Figure 18.- Effect of acceleration on pit diameter and pit density at maximum burning rate. Throat sized for nominal chamber pressure of 4.14 MN/m^2 (600 psia).
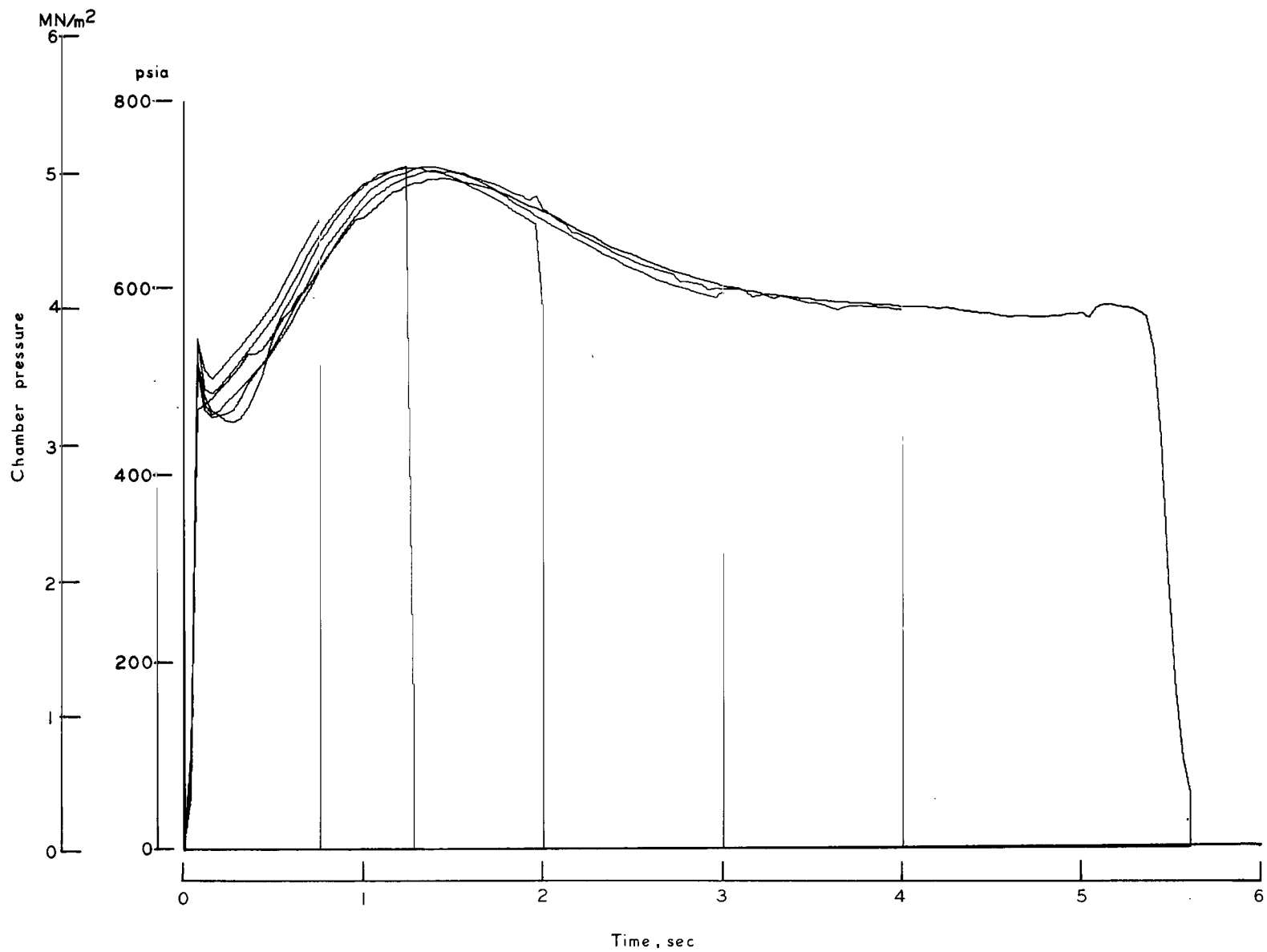
Figure 19.- Extinction test pressure histories at 140g.

Static; DB=1.0in.(25.4 mm)

DB=0.24in.(6.1mm);0.75sec
Rise

DB=0.39in.(9.9mm);1.25sec
Peak

DB=0.78in.(19.8mm);2.00sec
Decay

DB=1.16in.(29.5mm);3.00sec
Decay

DB=1.52in.(38.6mm);4.00sec
Equilibrium

25.4mm
(1.0in.)
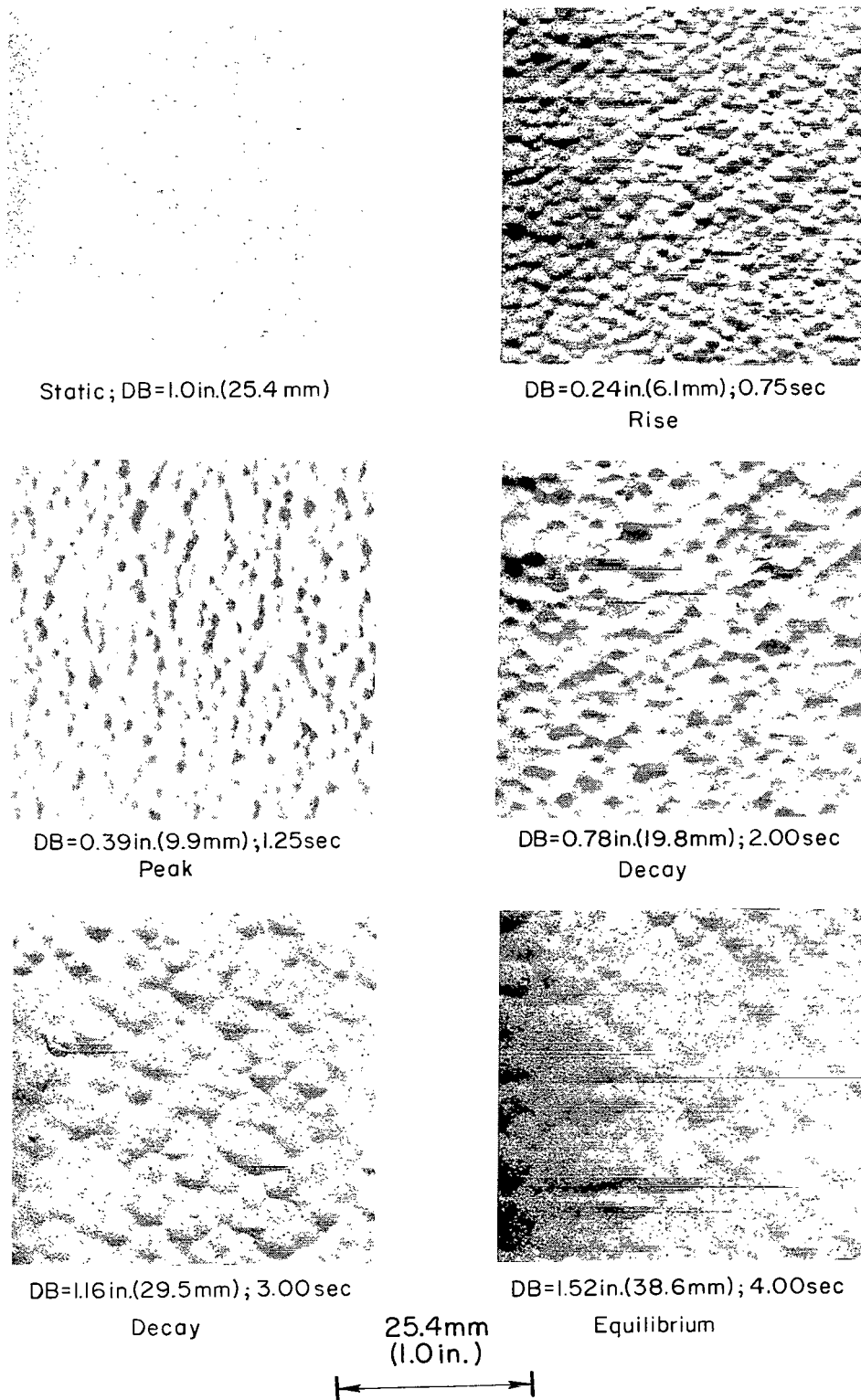
Figure 20.- Photographs of extinguished propellant surface at 140g and pressures
shown in figure 19.
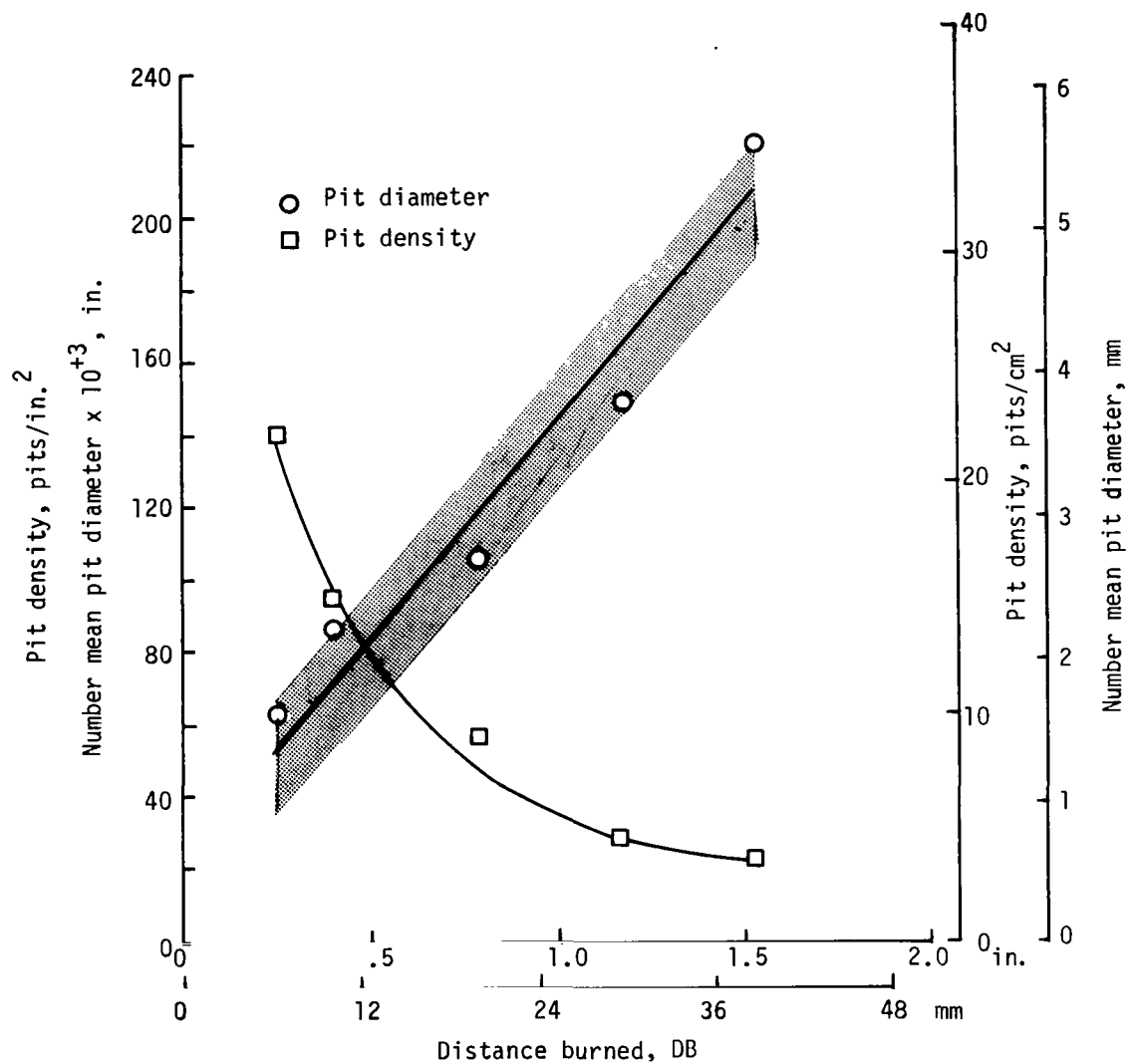
Figure 21.- Effect of distance burned on pit diameter and pit density at 140g normal acceleration and nominal chamber pressure of 4.14 MN/m^2 (600 psia).
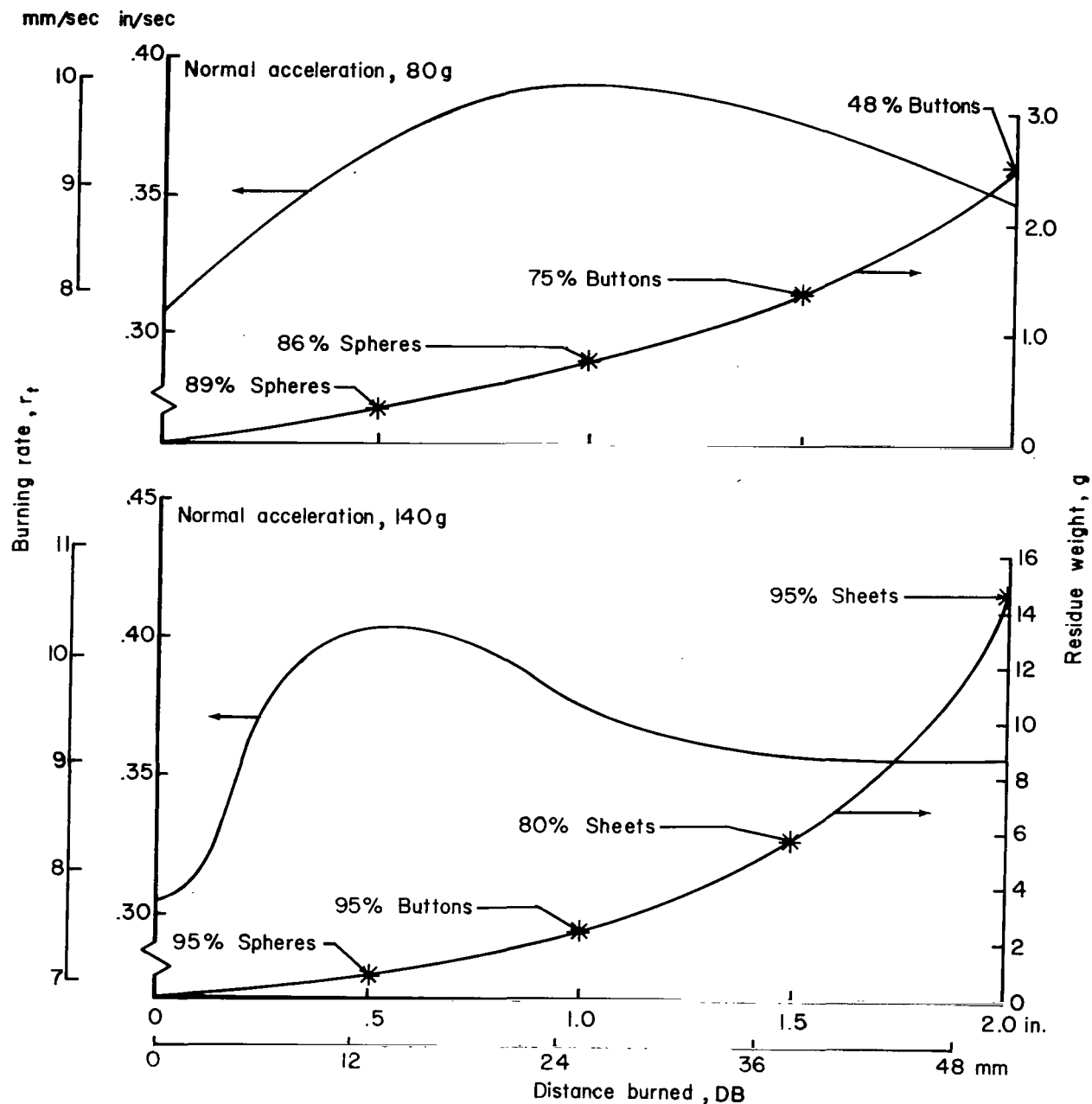
Figure 22.- Correlation of burning-rate and residue characteristics.

*"The aeronautical and space activities of the United States shall be
conducted so as to contribute . . . to the expansion of human knowl-
edge of phenomena in the atmosphere and space. The Administration
shall provide for the widest practicable and appropriate dissemination
of information concerning its activities and the results thereof."*

— NATIONAL AERONAUTICS AND SPACE ACT OF 1958

NASA SCIENTIFIC AND TECHNICAL PUBLICATIONS

TECHNICAL REPORTS: Scientific and technical information considered important, complete, and a lasting contribution to existing knowledge.

TECHNICAL NOTES: Information less broad in scope but nevertheless of importance as a contribution to existing knowledge.

TECHNICAL MEMORANDUMS: Information receiving limited distribution because of preliminary data, security classification, or other reasons.

CONTRACTOR REPORTS: Scientific and technical information generated under a NASA contract or grant and considered an important contribution to existing knowledge.

TECHNICAL TRANSLATIONS: Information published in a foreign language considered to merit NASA distribution in English.

SPECIAL PUBLICATIONS: Information derived from or of value to NASA activities. Publications include conference proceedings, monographs, data compilations, handbooks, sourcebooks, and special bibliographies.

TECHNOLOGY UTILIZATION PUBLICATIONS: Information on technology used by NASA that may be of particular interest in commercial and other non-aerospace applications. Publications include Tech Briefs, Technology Utilization Reports and Technology Surveys.

Details on the availability of these publications may be obtained from:

SCIENTIFIC AND TECHNICAL INFORMATION OFFICE

NATIONAL AERONAUTICS AND SPACE ADMINISTRATION
Washington, D.C. 20546